RESEARCH ARTICLE

ADVANCED
INTELLIGENT
SYSTEMS
Open Access

www.advintellsyst.com

Optimized Magnetically Docked Ingestible Capsules for Non-Invasive Refilling of Implantable Devices

Hind Al-Haddad,* Daniele Guarnera, Izadyar Tamadon, Lorenzo Arrico, Giulia Ballardini, Francesco Mariottini, Alessio Cucini, Simone Ricciardi, Fabio Vistoli, Maria Isabella Rotondo, Daniela Campani, Xuyang Ren, Gastone Ciuti, Benjamin Terry, Veronica Iacovacci, and Leonardo Ricotti*

Automated drug delivery systems (ADDS) improve chronic disease management by enhancing adherence and reducing patient burden, particularly in conditions like type 1 diabetes, through intraperitoneal insulin delivery. However, periodic invasive refilling of the reservoir is needed in such a class of implantable devices. In previous work, an implantable ADDS with a capsule docking system is introduced for non-invasive reservoir refilling. Yet, it encounters reliability issues in manufacturing, sealing, and docking design and lacks evidence on intestinal tissue compression effects and chronic in vivo data. This work proposes an optimization of the different components featuring this ADDS. The ingestible capsule is designed, developed, and tested following ISO 13485, exhibiting high insulin stability and optimal sealing for six days in harsh gastrointestinal-like conditions. A magnetic docking system is optimized, ensuring reliable and stable capsule docking at a clinically relevant distance of 5.92 mm. Histological tests on human intestinal tissues confirm safe capsule compression during docking. Bench tests demonstrate that the integrated mechatronic system effectively docks capsules at various peristalsis-mimicking velocities. A six-week in vivo test on porcine models demonstrates chronic safety and provides hints on fibrotic reactions. These results pave the way for the further evolution of implantable ADDS.

1. Introduction

Over the past few decades, there has been a remarkable increase in the prevalence of chronic diseases that require medical care,[1] for example., chronic pain management,[2] pulmonary arterial hypertension,[3] and type 1 diabetes (T1D).[4] This upward trend results in a growing proportion of the population with persistent disabilities.[5] The standard treatments for these illnesses have low efficacy due to high drug dosage requirements and poor patient adherence. This results in disease progression, mortality, and increasing healthcare costs.[6,7] Automated drug delivery systems (ADDS) have the potential to enhance treatment efficacy for various chronic diseases significantly, since they enable precise drug delivery, diminishing or avoiding the need for patient intervention.[8]

Patients with T1D require insulin-replacement therapy as their pancreas cannot produce insulin due to the autoimmune destruction of pancreatic beta cells.[9] Continuous insulin delivery based on blood glucose levels using ADDS provides better glycemic control and reduces the risk of

H. Al-Haddad, D. Guarnera, I. Tamadon, X. Ren, G. Ciuti, V. Iacovacci, L. Ricotti
The BioRobotics Institute
Scuola Superiore Sant'Anna
Piazza Martiri della Libertà 33, 56127 Pisa, Italy
E-mail: hind.alhaddad@santannapisa.it; leonardo.ricotti@santannapisa.it

H. Al-Haddad, D. Guarnera, I. Tamadon, X. Ren, G. Ciuti, V. Iacovacci, L. Ricotti
Department of Excellence in Robotics & AI
Scuola Superiore Sant'Anna
Piazza Martiri della Libertà 33, 56127 Pisa, Italy

The ORCID identification number(s) for the author(s) of this article can be found under https://doi.org/10.1002/aisy.202400125.

I. Tamadon
Faculty of Engineering Technology
University of Twente
Drienerlolaan 5, 7522, NBEnschede, Netherlands

L. Arrico
Department of Chemistry and Industrial Chemistry
University of Pisa
Via Moruzzi 13, 56124 Pisa, Italy

G. Ballardini
Max Planck Institute for Intelligent Systems
70569 Stuttgart, Germany

F. Mariottini, A. Cucini, S. Ricciardi
WAVECOMM s.r.l
53034 Colle di Val d'Elsa, Italy

F. Vistoli
Division of General and Transplant Surgery
University of Pisa
56124 Pisa, Italy

complications compared to standard insulin self-injections.[10,11] Currently, subcutaneous (SC) insulin delivery is mainly used for ADDS. SC insulin delivery is widely used in commercial systems due to its patient-friendliness and convenience.[12–14] However, this route suffers from delayed insulin absorption and poor tolerability with sudden changes in insulin demand in a bolus state (an increase of blood glucose levels after meals), which needs meal announcements (inputs concerning the amount of carbohydrates assimilated in the meal), making precise control challenging.[15] Conversely, the most promising but relatively less explored insulin delivery route by commercial systems is intraperitoneal (IP) administration. IP delivery has demonstrated its superiority in terms of insulin pharmacokinetics and rapid insulin actions, thanks to the delivery location near the physiological one (near the portal vein). This offers a higher insulin concentration in the portal system than in the peripheral system, mimicking the natural pancreatic release strategy.[16] For those reasons, IP overcomes some limitations of the SC route, including but not limited to the risk of peripheral hyperinsulinemia and meal announcements.[16,17] Despite these advantages, its use in T1D treatment remains low (less than 1% of current insulin treatment) due to the invasiveness of currently available technologies.[18] Two commercial ADDS, the DiaPort System (Roche Diagnostics, F. Hoffmann-La Roche AG, Switzerland) and the Minimed 2007 (Medtronic Inc., USA), exploited the IP insulin delivery.[19] The use of the DiaPort System, which has a percutaneous port connected to a wearable insulin pump, is limited by infection risks at the implantation site.[20] Additionally, the secure affixation of the wearable device to the body poses practical challenges and can negatively impact many daily living activities.[12,21] To overcome these limitations, Medtronic Inc. introduced Minimed 2007, a fully implantable pump with a refillable reservoir with transcutaneous access. The device reservoir needed to be periodically refilled (approximately every 6–12 weeks) with an invasive procedure that could only be performed in a clinical setting. This implied high costs, risks of infection, and an overall unacceptable burden for patients.[22,23] A similar system (SynchroMed infusion system, by Medtronic Inc.) has also been used for the treatment of chronic pain through intrathecal drug release,[24] although similar limitations apply.

In this framework, our group proposed an innovative approach to refill a fully implantable system for automatic IP or intrathecal drug delivery. The system could be refilled non-invasively through an ingestible drug-carrying capsule, which was magnetically docked. Subsequently, the drug was aspirated from the capsule and delivered to the implanted reservoir.[25–28] This technology has the potential to enable TID patients to effortlessly maintain normoglycemia, thereby obviating the need for continuous meal announcements and treatment interventions, as well as preventing the need for invasive reservoir refilling procedures.

Despite interesting short-term results obtained, this technology needs improvements, especially concerning the refilling mechanism of the implanted reservoir using the ingestible capsule, which showed limitations. First, the stability of capsule docking needs to be improved: past system designs did not carefully consider the dimensions of healthy and pathological human tissues affecting magnetic force decay and did not address capsule tilting during punching. Also, tissue safety at the interface was not evaluated. Furthermore, the passive capsule structure was prototyped through manual molding and gluing, with poor repeatability and not guaranteed sealing. Insulin stability, capsule resistance to gastrointestinal fluids, and other aspects were also not considered. Furthermore, since the system was implanted for only a single day, the potential diverse effects of the surgical procedure, the interaction of the implant with the tissue, and the overall health of the animal models were not taken into account.

In addition to our group work, several examples of ingestible devices performing therapeutic actions in the gastrointestinal tract are reported in the state-of-the-art. Sun and colleagues introduced a small-scale capsule driven by external magnets, incorporating magnetic soft robotics into its design and equipping it with a flexible magnetic soft valve. The capsule facilitated controlled interactions with the gastrointestinal tract, enhancing drug release and sampling capabilities.[29] Srinivasan et al. developed a robotic ingestible drug delivery capsule to improve drug absorption in the small intestine by locally clearing the mucus layer and optimizing drug deposition.[30] Additionally, the Traverso research group explored the development of an injecting self-orienting millimeter-scale applicator for drug delivery via gastric submucosa injection[31–33] alongside a non-invasive oral microneedle injector for protein-based drug delivery in small intestine.[34] Terry et al. presented a capsule-delivered enteric drug-injection device, which deployed an osmotic pump and drug delivery needle through a tissue attachment mechanism within the small intestine, facilitating systemic drug delivery.[35] While these studies offer comprehensive insights into device functionality both in vitro and in vivo, challenges persist in capsule fabrication methods, adherence to medical device standards, the investigation of gastrointestinal enzymatic degradation effects on the capsule body, and sealing and standardized drug-filling procedures within the capsule.

This article aims to overcome these challenges and propose a robust and efficient capsule docking system. To achieve this goal, we introduced a novel capsule layout that exhibited compatibility with industrial manufacturing techniques and ensured insulin stability, resistance to gastrointestinal fluids, and softness (essential to allow a low punching force). Furthermore, the capsule design is thought to allow patients filling a sealed capsule with insulin effortlessly and securely, in sterile conditions, with no concerns regarding leakage after ingestion. Moreover, the docking system design was improved to achieve a high level of stability in capsule docking and ensure the biocompatibility of the

M. Isabella Rotondo
Division of Surgcal Pathology
Azienda Ospedaliero Universitaria Pisana
56126 Pisa, Italy

D. Campani
Division of Surgical Pathology
Department of Surgical, Medical, Molecular Pathology and Critical Area
University Hospital of Pisa
56124 Pisa, Italy

B. Terry
Mechanical Engineering Department
College of Engineering
Brigham Young University
Provo, UT 84602, USA

implanted device by incorporating magnets internally to the case without exposing them to tissues. Moreover, we took into account the specific anatomic alterations associated with T1D, specifically the potential increase in tissue thickness of the digestive tract,[36,37] which was an overlooked factor in previous studies. The article also provides preliminary validation of the system's safety by investigating the effect of compression stress and compression time due to capsule docking on human intestine tissues ex vivo. Additionally, a semi-automated mechatronic system was assembled and tested to validate capsule detection and docking in challenging scenarios, including ones featured by a large tissue thickness, and different capsule velocities mimicking different intestine peristaltic activities. Finally, a simplified version of the system was implanted in three pigs and monitored for six weeks. This allowed for validating the surgical procedure and device safety, assessing its impact on intestinal peristaltic movements and related health issues.

2. Results and Discussion

2.1. System Overview

The concept of the refilling system targeted in this work is schematically presented in **Figure 1**. The patient is instructed to periodically ingest a drug-carrying capsule that passively travels through the gastrointestinal (GI) tract. Once the capsule reaches the implanted device, it undergoes a docking process, followed by
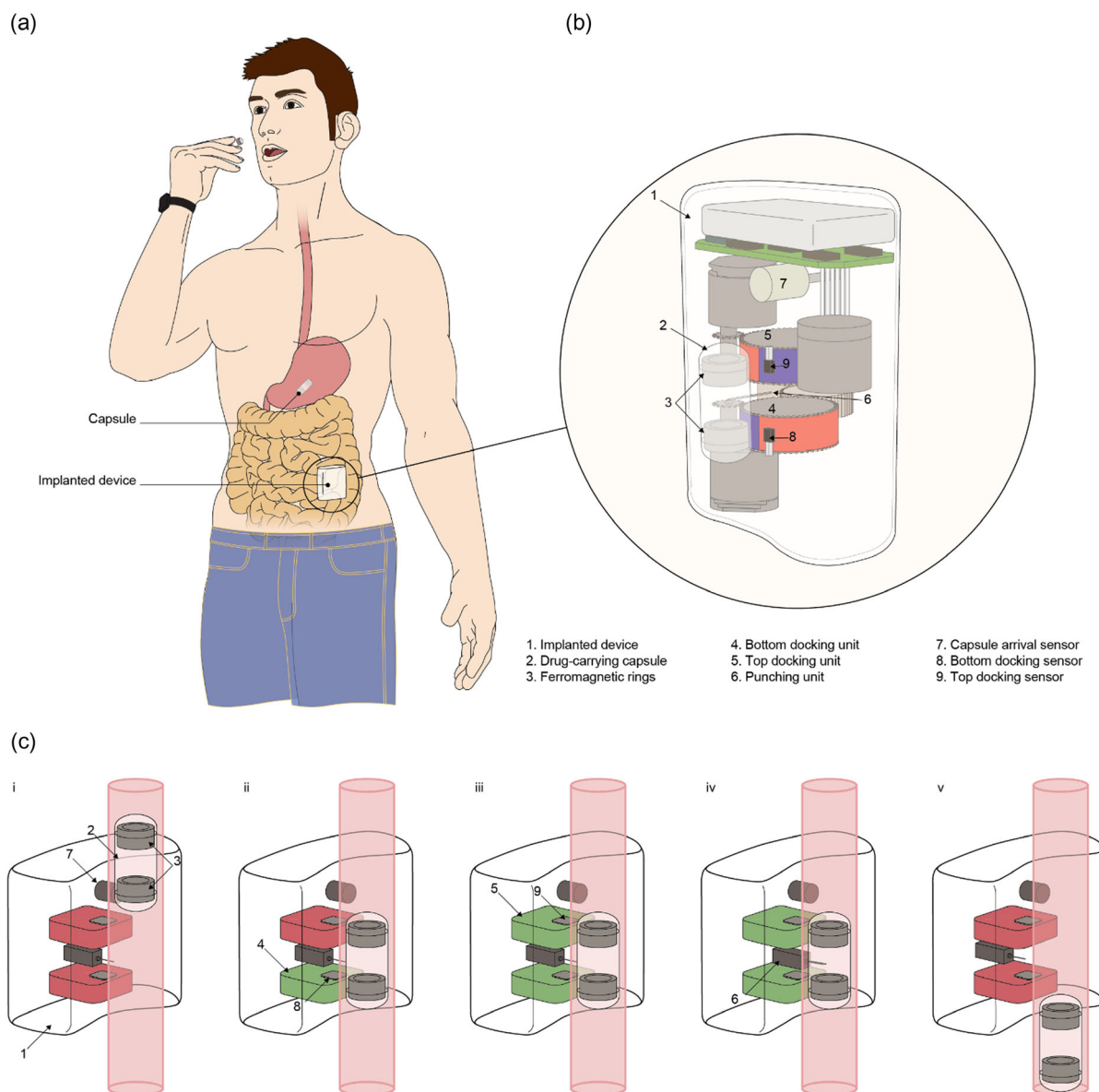
Figure 1. System overview and operation sequence. a) Position of the implanted device and representation of the ingestible capsule. b) CAD of the whole system, with its components. c) Depiction of the sequential activation steps for the capsule docking procedure: dock, punch, and release of the capsule following the refilling process (i–v). Green = activated magnetic unit; Red = deactivated magnetic unit.

1. Implanted device
2. Drug-carrying capsule
3. Ferromagnetic rings
4. Bottom docking unit
5. Top docking unit
6. Punching unit
7. Capsule arrival sensor
8. Bottom docking sensor
9. Top docking sensor

piercing with a needle, to extract the drug from the capsule and transfer it to a reservoir (not addressed in this study). The implanted device 1) is placed in an extraperitoneal pouch between the costal margin and the iliac crest and surgically interfaced with the third jejunal loop in the left quadrant of the abdomen, as in Figure 1a.[38] The refilling system is shown in Figure 1b, and it includes i) a drug-carrying capsule 2) embedding two ferromagnetic rings 3) enabling the magnetic docking; ii) a docking system made of two magnetic units [bottom 4) and top 5)] that are activated/deactivated by motors and dedicated force transmission mechanisms, to dock/undock the capsule; iii) a punching unit 6) that ejects a needle to pierce the capsule wall, subsequently enabling the drug to be transferred to the implanted device; vi) an inductive sensor 7) to detect the capsule arrival (capsule arrival sensor), and two Hall effect sensors (8 and 9) (one per magnetic unit), to monitor the success of the docking phase (docking sensors). The capsule docking strategy presented in this work is based on the following steps (shown in Figure 1c): 1) The capsule arrival sensor detects the capsule approach, and the bottom unit of the docking system turns on (Figure 1c-i). 2) The capsule is blocked by the magnetic attraction between the bottom magnetic unit and the capsule's bottom ring. The docking sensor of the bottom unit provides feedback to activate the top magnetic unit (Figure 1c-ii). 3) The top magnetic unit of the docking system turns on to attract the capsule's top ring. The docking sensor of the top unit confirms the successful docking and triggers the punching unit to eject the needle (Figure 1c-iii). 4) The needle punches the capsule (Figure 1c-iv). 5) The needle retracts, and the two docking units are turned off. Consequently, the capsule can be undocked and expelled (Figure 1c-v).

The aforementioned components and their performance are described in detail in the following sections.

2.2. The Drug-Carrying Capsule

The capsule is a drug cargo designed to be a passive structure traveling along the GI tract toward the implanted device through peristalsis. As detailed in the following sections, the capsule's primary function is safely carrying the drug across the GI tract environment for an extended period while facilitating the aspiration of the drug by the implanted device. The capsule is thought to be used regularly by the patient and thus needs to pass through the human GI tract without complications. The capsule dimensions are 11 mm in diameter and 30 mm in length, resembling the endoscopic capsule dimensions already used in the clinic.[39] Moreover, the dimension was chosen with an 11 mm diameter, considering that the resistance of capsule transit in the gastrointestinal tract is more affected by diameter than capsule length.[40] Thus, our selected capsule diameter aligns with the size of standard ingestible endoscopic capsules[41] and ingestible sensors.[42–44] The capsule was devised considering reliable fabrication and assembly procedures compatible with ISO 13485 (quality management systems for medical devices) to facilitate future regulatory pathways. In particular, injection molding was selected as the fabrication method. This method is widely used in medical device manufacturing due to its effectiveness in achieving high quality and repeatability, while being cost-effective.[45]

The capsule components are depicted in **Figure 2**a. They were: i) a bi-component body, which forms a unified unit after sealing, constituting a reservoir to house the drug; each body has dedicated slots to enclose the ferromagnetic rings; ii) two ferromagnetic rings that allow magnetic anchoring to the device; iii) a self-sealing septum that allows filling the assembled capsule with the drug, preventing any leakage in (or out); iv) two caps to provide a hermetic closure.

This capsule's design considered the assembly and sealing process of the capsule components. The assembly of the capsule body was a straightforward procedure that relied on the geometrical matching between the different components coupled with subsequent sealing actions, as depicted in Figure 2a-i–vi. In particular, the foreseen assembly steps can be summarized as follows: the top part of the capsule was assembled by inserting the septum in the cap, followed by assembling the ring with the cap, and then the adhesive agent was applied to the edge of the cap top and bottom part, then inserted carefully in the body of the capsule as shown in Figure 2a-i–iii. The adhesive was avoided on the internal surface of the cap to facilitate the capsule body collapse during drug aspiration. The bottom part of the capsule followed the assembly procedure as the top one, except for the absence of the septum in the cap (Figure 2a-iv,v).

After the adhesive was fully cured, the top and bottom parts of the capsule structure were joined together. The adhesive was carefully dispensed on the internal surface of the bottom capsule body. Immediately after, the capsule's top part was assembled (Figure 2a-vi).

2.2.1. Capsule Shell (Body and Cap): Material Selection

Various factors drove the selection of the capsule material. The shell material had to resist the GI fluids and, at the same time, be soft enough to allow the piercing by the needle. Biocompatibility and compatibility with the injection molding technique were other essential requirements. Additionally, the material should ensure insulin stability for the period needed to reach the implantation site.

Four materials were considered for the capsule shell: three polypropylene-based (PP) thermoplastic elastomers (TPE Kraiburg, TPE Versaflex, TPE Nevifood) and polyvinyl chloride (PVC, TPV Compound). The materials' properties and FTIR spectra are reported in Table S1, and Figure S1, Supporting Information, respectively. These materials, commonly used in medical devices, were considered due to their versatile mechanical properties and the wide range of hardness values covered. Moreover, they can be fabricated through injection molding, targeting low thickness.[46] Specific tests were performed to evaluate the materials according to the above-mentioned requirements. The results are described in the following sections.

Degradation Test: As mentioned, capsule material must resist the GI environment to prevent drug contamination or leakage during transit toward the implanted device. The selected materials belonged to two classes of polymers (PP and PVC) with saturated C—C chains, which are well-known for their stability to the hydrolysis at low temperatures in the dark, i.e., in conditions resembling those of the digestive systems.[47–50] Nevertheless, the degradation tests were carried out to assess some unexpected
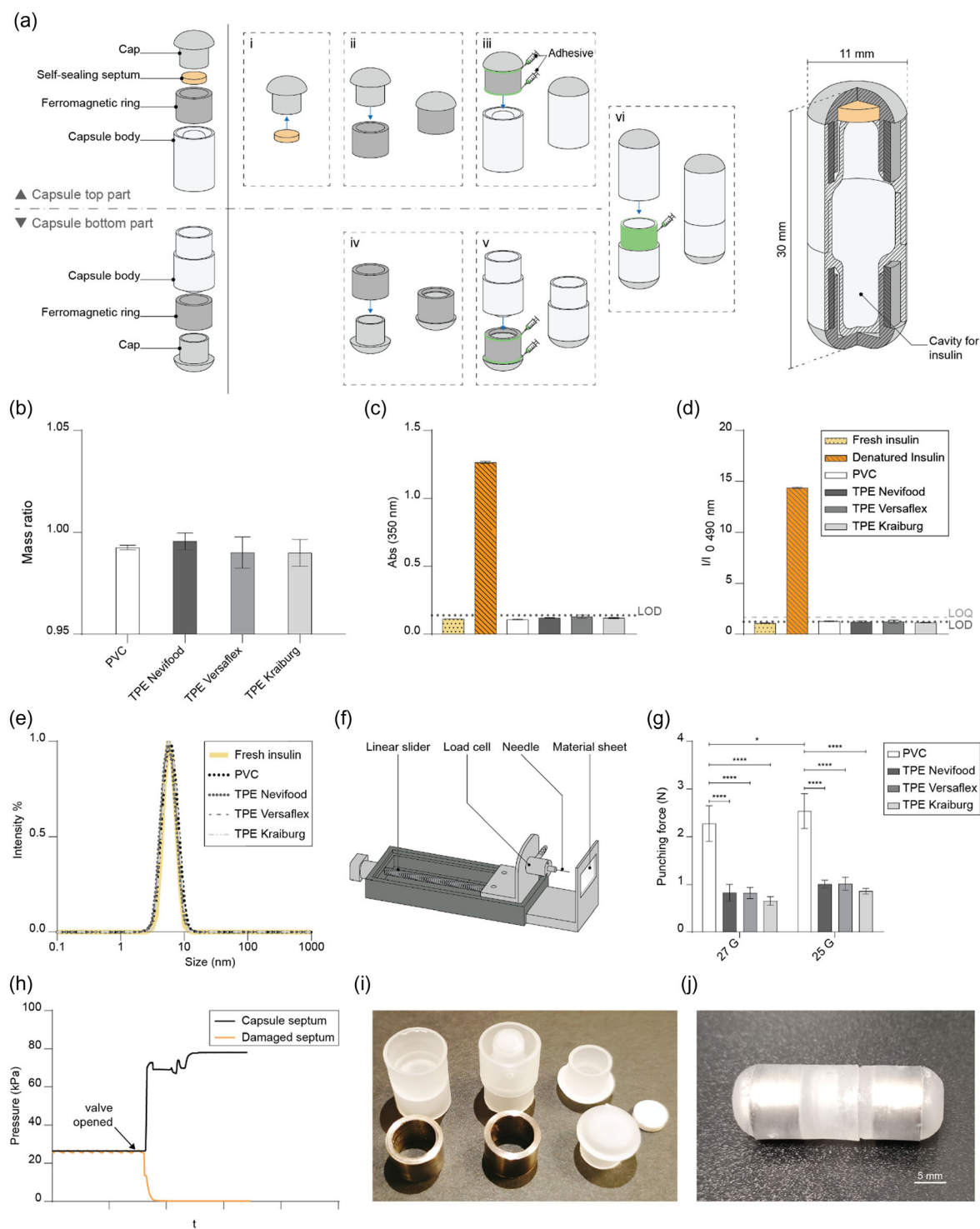
Figure 2. Capsule design, material characterization, and fabrication. a) Depiction of capsule main components: on the left, an exploded view; in the middle (i–vi), the stepwise assembly and adhesive sealing process leading to the complete capsule structure; on the right, a partial cross-section of the fully assembled capsule. Green = adhesive zone. b) Outcome of sequential treatment of the four capsule materials tested with simulated gastric fluids for one day and simulated intestinal fluids for five days. c–e) Outcomes of insulin stability using turbidimetry, fluorescence, and dynamic light scattering measurements techniques, respectively. LOD = limits of detection, LOQ = Limit of quantitation. f) Depiction of the setup used for measuring the force needed for punching the different candidate materials for the capsule shell. g) Outcome of punching force measurements obtained with 0.6 mm-thick sheets using 27 and 25 G needles for PVC and three TPE Materials (Nevifood, Versaflex, Kraiburg) with a hardness of 76, 60, 54, 43 shore A, respectively. * = $p < 0.05$; **** = $p < 0.0001$. h) Pressure sensor response during the leakage test applied to the capsule septum. i) Fabricated capsule components. j) Picture of the assembled capsule.

**ADVANCED
SCIENCE NEWS**

www.advancedsciencenews.com

**ADVANCED
INTELLIGENT
SYSTEMS**

www.advintellsyst.com

behavior in the stability of the selected materials. This behavior may arise from impurities or additives in their formulations and enzymes in the digestive fluids. The digestive system presents different chemical properties, such as pH and enzymatic composition that change along the GI tract. The samples of each material were thus incubated for one day in simulated gastric fluid (SGF, pH 1.2) and for five days in simulated intestinal fluid (SIF, pH 6.8). These extended times were considered the worst-case scenario, taking into account endoscopic capsule transit times.[51,52] The materials' mass was measured before and after incubation to assess if degradation or leakage of additives occurred. At the end of the test, no mass loss was observed for all samples in both fluids, as shown in Figure S2, Supporting Information. Furthermore, selected materials were also tested sequentially: first in SGF fluid for one day and then in SIF fluid for five days. Also, in this case, the treatments did not affect the mass of the candidate materials, where the mass ratio remains close to one for all the tested materials (Figure 2b). This result confirmed that the selected materials did not degrade in the digestive system for the tested period, ensuring the capsule's integrity. The limited availability of chemical information on the materials used in the gastroenterology field often hinders the comprehensive identification of suitable materials for application in the GI tract. The scarcity of data regarding the chemical composition of devices is due to limited disclosure by manufacturers and a lack of interest by physicians, in this matter.[53] The PVC material belongs to the same family as the material used in feeding tubes,[54] while no knowledge is available about the behavior of PP-based TPE in the GI tract. To the author's knowledge, no studies have been conducted to assess the effect of digestive fluids on different brands with different hardness values of TPE materials. Our results thus constitute a piece of novelty, which could help other authors interested in using such materials for GI-related applications.

Insulin Stability Test: As mentioned, the proposed non-invasive refilling system could be beneficial for the automated release of a series of drugs targeting different chronic diseases. In the case of T1D treatment, the target drug is insulin. In this case, a specific test is required to ensure insulin stability within the capsule. Indeed, insulin tends to aggregate, forming amorphous or fibril-like structures that are not biologically active.[55] Such larger molecular aggregates can affect the implanted device's functioning and trigger unfavorable immune reactions.[56] The aggregation kinetics strongly depends on factors such as insulin concentration, excipients, pH, ionic strength, temperature, and agitation, but also on the material that goes in contact with the hormone.[57–59] We selected Insuman Infusat 100 IU for our tests, a phenol-stabilized insulin formulation to enhance insulin resistance against thermal aggregation, thereby partly preventing protein aggregation.[60] However, insulin behavior in contact with the different materials could not be predicted, and thus tests were needed. The formation of aggregates was evaluated after storing the insulin inside the capsules made of different materials, kept in continuous agitation and at 37 °C, replicating the intracorporeal conditions for 24 h. The capsule shells were hence filled with Insuman Infusat 100 IU and were incubated for 24 h, i.e., a period three times longer than the time needed for the capsule to reach the implanted device placed on the third loop of the jejunum.[51] After that, the insulin was retrieved from the capsule

and analyzed. To check for the presence of high molar mass aggregates and amyloid-like structures and to obtain information on the protein size distribution, turbidimetry, fluorescence, and dynamic light scattering (DLS) were used.[61,62] The results of the three analyses are shown in Figure 2c–e. All tested materials did not trigger any observable insulin aggregation during the test period. Fresh insulin (taken from the original cartridges stored at 4 °C) and capsule-incubated insulin responded similarly to turbidimetry, fluorescence, and DLS tests. In particular, turbidimetry and fluorescence values obtained from fresh insulin and incubated insulin laid in the proximity of the limits of detection (LOD) of the two methods, indicating that no significant amount of higher molar mass aggregates (Figure 2c) and amyloid-like fibrils (Figure 2 d) was present in the insulin stored inside the capsules. Regarding DLS results (Figure 2e), the protein size distributions are almost superimposable, excluding the presence of any insulin aggregation. No information was available in the literature about the stability of the specific insulin formulation used in this study in contact with the selected materials. In the case of different insulin formulations, PVC and, to a lesser extent, PP showed some tendency to absorb insulin,[63] which may facilitate the formation of amyloid fibrils.[64] Our results thus clarify that the four materials tested can be considered safe for contact with Insuman Infusat 100 IU for 24 h.

Material Resistance to Punching: The drug transfer from the capsule to the device is devised through a needle that pierces the capsule and extracts the drug by aspirating it. The force needed to punch the capsule was set as a final criterion for selecting the proper material for the capsule. Smaller force values would be more desirable since a smaller motor would be needed to activate the needle, with less risk of damaging the needle tip during punching in the long run. Furthermore, smaller punching force values would also imply the need for smaller magnetic attraction forces to mitigate undesired tilting or detachment of the capsule during the punching event. Samples of the selected materials with a thickness of 0.6 mm were tested. Two needle sizes (27 and 25 G) were considered (see Section 2.4). The needles were mounted on a load cell and actuated by a motorized linear stage (Figure 2f) and Movie S1, Supporting Information.

The punching forces required by the tested materials for both needle sizes are shown in Figure 2g. No statistically significant difference in the punching force was observed among the TPE materials for both needle sizes. For the 27 G needle, the obtained force values for TPEs Nevifood and Versaflex were similar, measuring 0.83 ± 0.18 N and 0.82 ± 0.12 N, respectively. Similarly, when the 25 G needle was used, the punching force increased by around 21% compared to the 27 G needle for both materials. The TPE Kraiburg exhibited lower force values, measuring 0.66 ± 0.09 N and 0.86 ± 0.12 N for the 27 G and 25 G needles, respectively. A significant difference was observed when comparing PVC with TPEs. PVC exhibited the highest hardness value of 76 Shore A, resulting in higher punching forces for both needle sizes ($p < 0.0001$). The effect of needle size is noticeable in the case of PVC, where the punching force increased with needle size, from 2.27 ± 0.37 N for the 27 G needle to 2.54 ± 0.37 N for the 25 G needle ($p < 0.05$). These findings are consistent with previous studies showing an association between increased punching force and the resistance encountered by the needle's

tip during the piercing event, attributable to both the larger needle size and the greater hardness of the material.[65]

At the end of this test, TPE Kraiburg, with a wall thickness equal to 0.6 mm, was finally selected for the capsule body and caps since it showed no degradation in GI fluids, no insulin stability issues, and it required the smallest punching force.

2.2.2. Self-Sealing Septum

The capsule included a self-sealing septum placed between the caps and the body, as shown in Figure 2a. This element, commonly used to seal medicinal vials, enabled the filling of pre-sealed capsules and prevented any leakage that could lead to drug infiltration and contamination. A thin rubber silicone septum with a thickness of 1.5 mm was chosen to minimize the space occupied by the septum while maintaining effective sealing. The self-sealing properties of the septa were assessed by puncturing them with 30 G needles selected for the capsule filling system (Figure S3 and Movie 2, Supporting Information). These septa were then enclosed in a dedicated setup and subjected to increasing pressure values, monitored through a pressure sensor. Contamination of a white filter paper was also checked to evaluate leakages, as depicted in Figure S4a, Supporting Information. The minimum pressure considered was 30 kPa to mimic the peristaltic pressure in the digestive tract.[66] No leaks were detected by the pressure sensor for values of pressure up to 70 kPa, as shown in Figure 2h, and no contamination of the white paper was qualitatively observed (Figure S4b, Supporting Information). In comparison, a similar test was conducted on a damaged septum. In this case, the pressure signal dropped quickly to 0 kPa (Figure 2h), and consistent leakage was observed in the white filter paper (Figure S4c, Supporting Information). These findings align with earlier research that utilized ultrathin septa for micro-implantable drug delivery systems featuring refillable reservoirs despite the variation in septum materials. Previous studies demonstrated that a septum enables leak-free refilling under high pressure, even after multiple piercings with non-coring needles of size 30 G.[67] This suggests that even a thin septum with self-sealing capability can sustain leak-free refilling. Our results show for the first time the possibility of applying such a paradigm to an ingestible capsule. This finding may have important implications since smart ingestible devices to deliver drugs along the GI tract have gained increasing importance in recent years.[33,68–71] Proposing a reliable and clinic-compatible way to fill them once sealed can actually increase their reliability and impact in the future.

2.2.3. Ferromagnetic Rings

The drug-carrying capsule also included two ferromagnetic rings to allow stable magnetic anchoring to the device.[38] The rings were made of high-permeability alloy (Alloy 50, Ed Fagan Inc. UK) and were placed internally, enclosed in lodges within the capsule body (Figure 2a), to avoid the release of metallic ions in the GI environment, which could raise toxicity issues.[72] Such a design maximizes capsule biocompatibility, which was an overlooked factor in previous studies.[27,28,38] The rings' height was equal to 7 mm, and the separating distance between the rings

was set to 10 mm. These dimensions derived from considerations that emerged during docking unit dimensioning (see Section 2.3).

2.2.4. Assembled Capsule: Fabrication, Sealing, and Testing

Capsule Shell Fabrication: Capsule production was carried out using injection molding and TPE Kraiburg as the constitutive material. The overall capsule features are reported in Table S2, Supporting Information. The mold used for capsule fabrication is shown in Figure S5, Supporting Information. The internal cavity of the capsule was designed without any sharp edges to minimize drug aggregation. The overall internal volume hosting the drug was 780 μL. The fabricated capsule components are shown in Figure 2i. The fully assembled capsule is shown in Figure 2j.

The overall features of the capsule developed in this study were compared with those reported in previous similar research[28] and other ingestible capsules documented in the state-of-the-art. Such a comparison, detailed in Table S3, Supporting Information, demonstrated that our capsule exhibits superior performance in several key aspects. Notably, it outperforms existing models in terms of material stability in the presence of gastrointestinal fluids, as well as insulin stability once kept in contact with the capsule material. These latter two parameters, particularly insulin stability, have not been thoroughly addressed in prior studies involving drug-loading ingestible capsules, underscoring the innovative aspects of our design and its potential impact on the field. Furthermore, a careful measurement of the thickness of the intestinal tissues in contact with the capsule is reported in our work (see Section 2.3). This aspect is also often neglected in the state-of-the-art, and it is subjected to high variability, depending on the specific location. Our detailed analysis of the jejunum tissue constitutes evidence that can be useful to future studies focusing on such a district.

Capsule Sealing and Testing: The assembled capsules were sealed using a Loctite 4902 cyanoacrylate medical adhesive. This material was chosen due to its ease of use and compatibility with flexible medical devices. The efficacy of this adhesive to seal TPE Kraiburg was evaluated through a tensile test performed on two samples of TPE bonded together, forming a single lap joint structure (Figure S6a, Supporting Information). The adhesive strength was measured before and after immersing the bonded sheets in digestive fluids (SGF for five hours and sequentially SIF for sixteen hours) to understand the effect of digestive fluids on the sealing strength. In both cases, the tensile tests revealed that the failure occurred due to the material, not the adhesive bonding junction (Figure S6b, Supporting Information), indicating that the adhesive was highly effective in bonding the capsule materials. There was no significant difference in failure stress-strain between the samples treated with digestive fluids (rupture stress: 1.90 ± 0.36 MPa, elongation at break; $403.9 \pm 36.6\%$, $N = 3$) and the samples without treatments (rupture stress: 1.91 ± 0.27 MPa, elongation at break; $469.5 \pm 68.4\%$, $N = 3$). These findings are consistent with previous studies regarding the influence of digestive fluids on adhesive behavior.[73] Also, in our case, the digestive fluids did not affect the bonding strength. However, we show for the first time the performance of the Loctite 4902 cyanoacrylate medical adhesive applied to PP-based TPE materials

**ADVANCED
SCIENCE NEWS**

www.advancedsciencenews.com

**ADVANCED
INTELLIGENT
SYSTEMS**

www.advintellsyst.com

(typically challenging to bond),[74] which was not reported in the state-of-the-art.

The sealing ability and the integrity of the assembled capsule were then assessed. The test was performed by replicating as much as possible realistic environmental conditions in terms of surrounding fluids and dynamic loads applied. Three capsules were assembled, sealed as mentioned earlier (Figure 2a), and left for at least 24 h for complete adhesive curing. Subsequently, the capsules were filled with dyed water (water with 0.006 M fluorescein sodium) using the filling system shown in Figure S3, Supporting Information. The capsules were then immersed in SGF for one day and then in SIF for five days at 37 °C under continuous agitation. After this treatment, the samples underwent a one-day-long static compression test (pressure ≈ 21 kPa), as shown in Figure S7, Supporting Information. No leaks were observed over the whole static compression period. A dynamic compression load was then applied to the capsules (>300 cycles) with a pressure higher than 40 kPa. Although the pressures were higher than those found in the intestine,[75,76] the capsules showed no leakage. The dynamic compression test is shown in Movie S3,Supporting Information. Sealed capsules were qualitatively compared to unsealed ones (negative controls), Movie S4, Supporting Information. The capsule was effective in preventing dye leakage even after prolonged immersion in simulated GI fluids and when exposed to high pressures, confirming the successful functionality of both the sealant agent used and the septum.

A full evaluation of capsule integrity and safety for frequent ingestion will be the object of a future pilot clinical trial. In future evolutions of the systems, a trade-off (driven by acceptability) should be searched between capsule size (the smaller, the better to facilitate ingestion) and ingestion frequency (the larger the capsule, the less frequent ingestion needed).

2.3. Docking System

As depicted in Figure 1, the capsule traveling through the GI tract must be magnetically attracted by the implanted device, thanks to the activation of the docking system. It consists of two magnetic units, referred to as the bottom unit and the top unit. The bottom unit stops the capsule's navigation, while the top unit serves to stabilize it (in the ON condition), allowing reliable punching. After insulin aspiration, the magnetic units are deactivated, and the capsule is released (switching the magnets to the OFF condition).
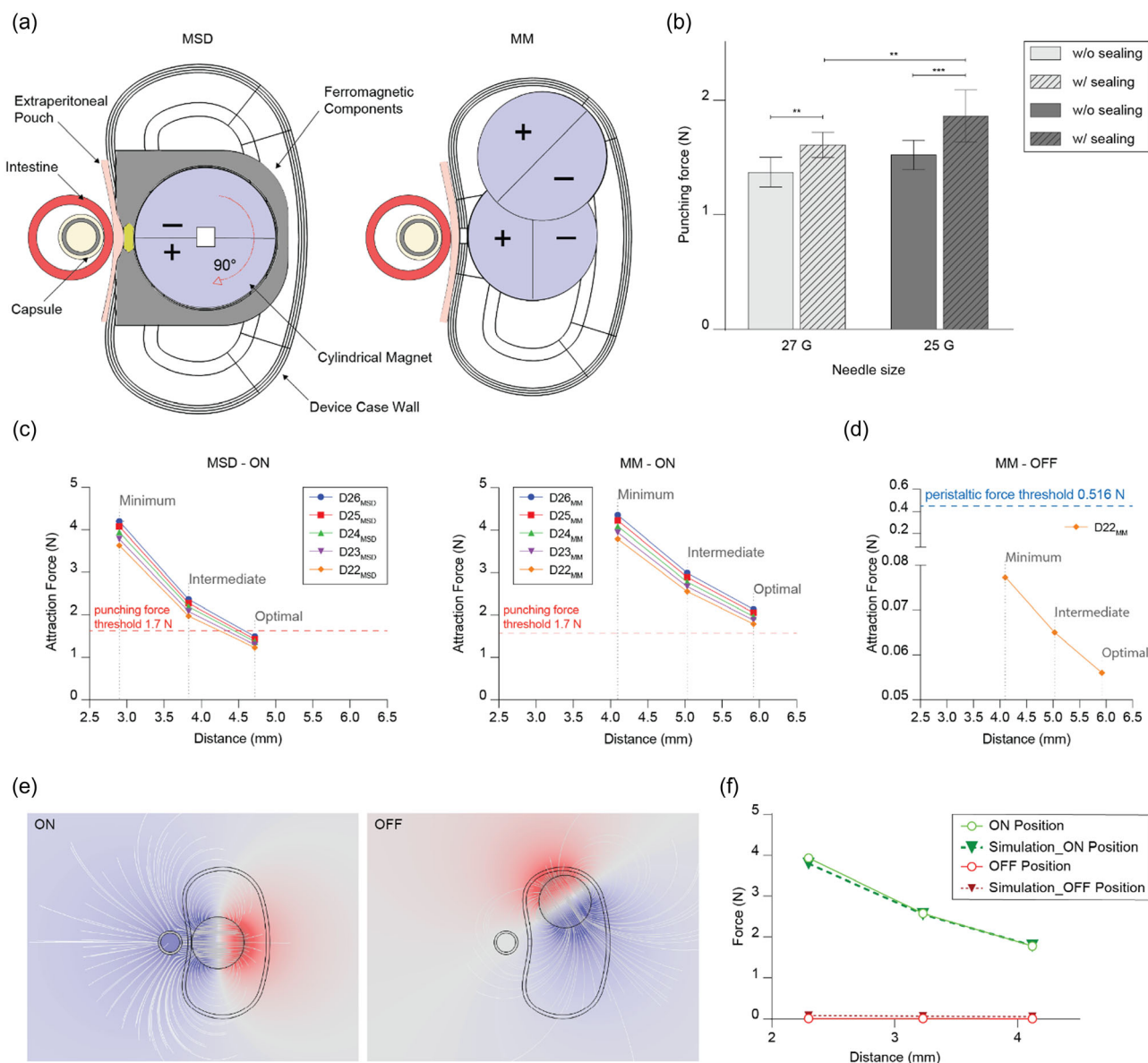
2.3.1. Docking System Design

The design of the magnetic docking system aimed to ensure a reliable attraction force and efficient transition from the ON to OFF conditions. The ON condition was designed to provide an attraction force to i) overcome the needle punching force in the opposite direction, and ii) prevent any tissue damage (see Section 2.3.2). On the contrary, the OFF condition should facilitate the natural detachment of the capsule under the effect of intestine peristalsis. Systems based on permanent magnets were preferred over electromagnets due to the lower power consumption required. Two different solutions were investigated for the magnetic units: i) one based on magnetic switchable devices

(MSDs), and ii) the other based on moving magnets (MMs). The authors had previously explored MSDs in the device's earlier version.[27,28,38] MSDs consisted of highly ferromagnetic components containing cylindrical permanent magnets (diametral magnetization, grade: N52). A 90° rotation of the magnets could activate or deactivate the magnetic attraction force toward a metallic target (in our case, the capsule's metallic rings). The ferromagnetic components enclosing the magnets were made of a high permeability nickel alloy (Alloy 50), which directed the magnetic field lines. MMs relied solely on the roto-translation of the magnets, enabled by a planetary gear mechanism. This mechanism brought the magnets closer to the capsule's route for the ON configuration and moved them away for the OFF configuration. The same magnets used in the MSDs solution were also used for the MMs solution. In both solutions, electric motors were employed to rotate the permanent magnets (in the MSDs solution) or move them (in the MMs solution), as described in Section 2.5. Both solutions, along with their working principles, are schematically shown in **Figure 3**a.

Setting the Minimum Attraction Force: To set the minimum necessary attraction force needed to anchor the capsule to the device firmly, we took into consideration the capsule punching force. In fact, without proper anchoring, the punching force exerted by the needle could displace the capsule, risking detachment and compromising drug aspiration. Thus, the punching force exerted by the needle on the assembled capsule was measured using a load cell connected to the needle. The test considered 25 and 27 G needles, and both sealed and non-sealed capsules were tested (capsule body wall thickness: 1.2 mm in fact, in the punching region, two layers are overlapped, each 0.6 mm thick). This allowed the evaluation of the role of the adhesive in modulating the punching force. The experimental setup used is shown in Figure S8, Supporting Information. The results of this test are shown in Figure 3b. The impact of the adhesive was evident for both needle sizes, resulting in a 14% increase in punching force for the 27 G needle (from 1.37 ± 0.13 N to 1.61 ± 0.11 N, $p \leq 0.01$) and an 18% increase for the 25 G needle (from 1.52 ± 0.13 N to 1.86 ± 0.23 N, $p \leq 0.001$). Furthermore, the needle size significantly influenced ($p < 0.01$) the punching force values recorded by the load cell. The 27 G needle was selected for magnet dimensioning due to its lower punching force values. The minimum necessary attraction force was set at 1.7 N (upper limit of the force values found for a 27 G needle puncturing the sealed capsule).

Magnet Dimensioning: The proposed solutions, MSDs and MMs, were compared in terms of attraction force in both the ON and OFF configuration through finite element (FE) numerical simulations. The objective was to determine the smallest magnet diameter surpassing the force threshold imposed by the punching force (1.7 N). The magnetic forces exerted by the docking systems were computed considering the distance between the magnets and the ferromagnetic rings. This distance was determined by the presence of soft tissues (intestine and extraperitoneal pouch), the capsule wall, and the device case wall (only in the case of MMs, which are completely internal to the device, while MSDs have a surface exposed to the external environment), as shown in Figure 3a. The intestinal tissue thickness was set at 1.50 ± 0.5 mm,[77] while the extraperitoneal pouch thickness was set at 1.28 ± 0.24 mm.[38] The intestinal tissue

ADVANCED
SCIENCE NEWS
www.advancedsciencenews.com

ADVANCED
INTELLIGENT
SYSTEMS
Open Access
www.advintellsyst.com

Figure 3. Docking system design and evaluation. a) Schematic representation of the capsule attracted to two docking systems investigated in this study: the MSD layout (MSD - left) and the MM layout (MM - right). b) The outcome of the punching test was carried out on the assembled capsule with and without an adhesive agent. c) Simulation results showing the attraction force between the docking system and the capsule at different distances and different magnet dimensions for the MSD (left) and the MM (right), compared to the threshold value (punching force with a 27 G needle). d) Simulation results in the OFF condition for the MM layout, with a magnet diameter of 22 mm and a height of 7 mm (the final selected magnet). e) Depiction of the magnetic field lines in the ON (right) and OFF conditions for the MM layout. f) Validation of the simulation outcomes through bench tests of the MM layout at different distances between the docking system and the capsule in both ON and OFF conditions.

thickness was increased by 30%, thus accounting for potential thickening in diabetic patients.[36,37] The device wall thickness was 1.2 mm, and the capsule wall was 0.6 mm (this is the capsule wall thickness in correspondence to the ferromagnetic rings). The sum of these layers defined three different operative distances: *minimum, intermediate, and optimal* (namely 2.90, 3.83, and 4.72 mm for the MSDs solution; 4.10, 5.03, and 5.92 mm for the MMs solution). By carefully considering all anatomical parameters, the obtained distance was significantly higher than the one considered in previous versions of the device.[27,28,38]

Consequently, larger magnets with diameters ranging from 22 to 26 mm were considered. Before comparing the docking solutions, the magnetic properties of the magnets were evaluated; results are shown in Figure S9, Supporting Information. The assessment is described in detail in the Experimental section.

The FE simulations were conducted through the AC/DC Module of COMSOL Multiphysics v6.0. The simulation results for the ON condition are shown in Figure 3c for the MSDs and MMs solutions. The estimated force included contributions from both the bottom and top magnetic units. As expected, the

ADVANCED
SCIENCE NEWS

www.advancedsciencenews.com

ADVANCED
INTELLIGENT
SYSTEMS
Open Access

www.advintellsyst.com

magnetic attraction force was significantly influenced by the distance in both the MSDs and MMs solutions. The impact of magnet diameter was more pronounced at the minimum distance: for both solutions, a diameter of 26 mm resulted in a gain of 0.6 N at the minimum distance and less than 0.3 N at the optimal distance, in comparison with the diameter of 22 mm. Concerning MSDs, even with the largest diameter (26 mm), this solution was unable to surpass the punching force threshold (red line) at the optimal distance (D26$_{MSD, optimal distance}$ = 1.24 N). Instead, the MMs exerted sufficient attraction force even with the smallest magnets, having a diameter of 22 mm (D22$_{MM, optimal distance}$ = 1.79 N). This force would allow the use of the device even in the worst-case scenario, corresponding to a gap equal to 5.92 mm. The MMs solution, with magnets having a diameter of 22 mm, represented the best trade-off between the force exerted on the capsule and the space occupied inside the device. Hence, they are a considerable advancement with respect to previous versions of the device.[27,28,38]

When comparing these results of MM's solution to the previous systems described in references,[27,28] it is clear that state-of-the-art systems cannot generate sufficient force at distances that are compatible with reliable in vivo use. Specifically, the attraction forces obtained using FE simulations applied to state-of-the-art systems at our target operative distances—minimum, intermediate, and optimal for MSDs—are 0.64, 0.36, and 0.22 N, respectively (Figure S10, Supporting Information). These values are significantly smaller than the required punching force, underscoring the superior performance of the docking system described in this work.

As mentioned, in the OFF condition, the residual attraction force provided by the magnets should be lower than the peristaltic force to facilitate capsule detachment. The attraction force provided by D22$_{MM}$ in the OFF condition was evaluated for all distances, and the results are depicted in Figure 3d. The force exerted by the magnets was equal to 0.077 N, sensibly smaller than the peristaltic force ($\approx$0.5 N),[78] thus guaranteeing capsule detachment. The attraction force in the OFF condition was also estimated for the MSD solution (D22$_{MSD}$), as shown in Figure S11, Supporting Information. In this case, the highest force was 2.5×10^{-5} N at the minimum distance (2.9 mm). Compared to the MM solution, the attraction force provided by the MSD solution in OFF condition is drastically weaker. This is due to the presence of ferromagnetic components surrounding the magnets, which close the field lines inside the circuit when the magnet is in the OFF condition. The stark contrast in the attraction force between the ON and OFF conditions is due to the distance and alignment of the magnetic field lines, as shown for the MMs solution in Figure 3e. In the ON condition, the capsule rings are affected by unidirectional field lines leading toward the center of the magnets, whereas in the OFF condition, the rings align with the magnetization diameter, resulting in the point of minimum force. To validate the computational results, the docking system with the MMs solution (magnet diameter of 22 mm) was fabricated and subjected to experimental measurements. The test is shown in Movie S5, Supporting Information. A comparison between the experimental measurements and the FE results in terms of attraction force for both ON and OFF conditions is shown in Figure 3f. The estimated forces properly matched the experimentally measured ones (mean error in the ON condition: 1.52%), thus confirming the validity of the simulation outcomes.

MSDs proposed in previous works[28] perform well in the ON condition when the target is within a range of 1–1.5 mm. However, at greater distances, which are likely in diabetic patients, the MSDs are unable to provide sufficient force, even with larger magnet dimensions. Consequently, the MMs solution is the most promising one. Another notable innovation is the presence of two metallic rings and two magnetic circuits, a feature already patented by the authors,[79] which allows the capsule to be punched at the center and blocked at its extremities, thus avoiding any rotational moment that could negatively impact insulin aspiration.

2.3.2. Tissue Damage Assessment

The compression stress exerted by the capsule, when magnetically docked, on the living soft tissues, such as the extraperitoneal pouch wall and intestine wall, can raise safety concerns. If excessive, in fact, this stress can severely compromise tissue integrity and result in significant trauma.

To estimate the stress induced by capsule pressure during magnetic anchoring, magneto-structural coupled FE simulations were used. These simulations considered the force exerted by MM solution, encompassing magnet diameters ranging from 22 to 26 mm. The MSDs solution was excluded from this evaluation due to its inability to generate the minimum required attraction force in the ON condition (see Section 2.3.1). The von Mises stress, as determined by FE simulations, exhibited an almost linear increase with magnet diameter, ranging from 63.6 to 77.2 kPa (**Figure 4**a). The 3D contour plots of tissue von Mises stress (Figure 4b, left) and capsule displacement (Figure 4b, right), obtained in the D22$_{MM}$ case, revealed stress concentration around the capsule position, with a peak near the metallic ring. Tissue compression (0.59 mm) facilitated closer proximity between the capsule and the device, increasing the magnetic attraction force from 1.8 to 2.1 N, thereby enhancing docking reliability.

To experimentally confirm the safety of the stress applied, tests were conducted using ex vivo human intestine samples. The samples were treated using a setup that applied a pressure of 80 kPa, similar to the estimation derived from FE simulations, but increased by a safety factor of $\approx$10%. A depiction of the setup is shown in Figure 4c, while Figure 4d shows a picture of the test conducted on freshly excised tissues. Images show the samples marked with Indian ink, in correspondence of the pillars. A video of this experiment is shown in Movie S6, Supporting Information. Different time intervals (10 s, 2, 5, and 10 min) were considered, compatible with the time required by our application ($\approx$2 min are needed for the whole docking and refilling procedure). Histological examinations performed on the compressed samples, along with positive and negative controls, revealed that even the worst-case scenario (10 min) resulted only in superficial layer damage, sparing the inner layers and overall maintaining tissue health, while no damage was observed for tissues compressed for less than 5 min (Figure 4e). The test was repeated two times using samples derived from two different donors. The overall results are shown in Figure 4f, in which the damage of the mucosa sub-layers is reported for each load and each time-point. Overall, these results demonstrate the safety
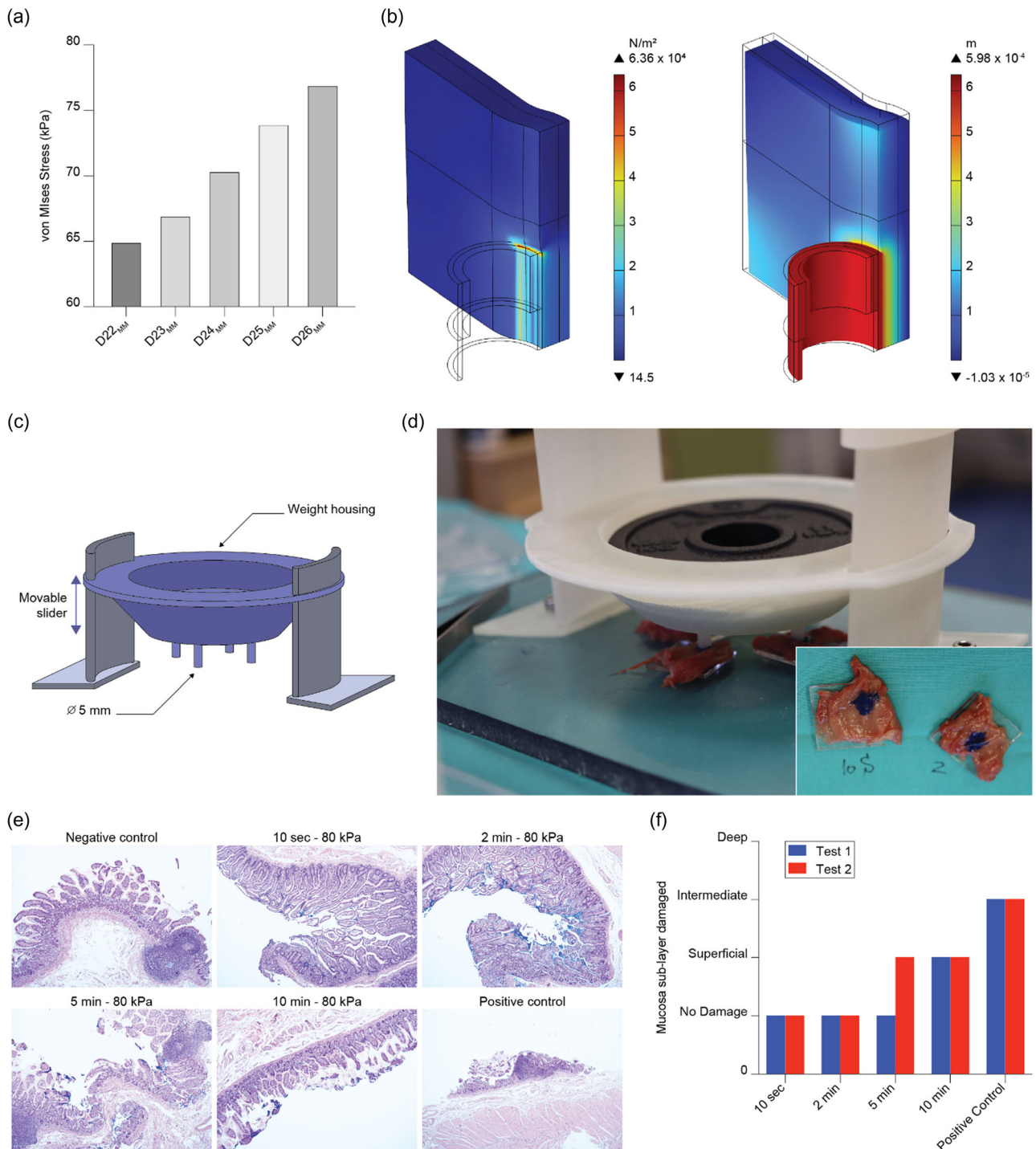
Figure 4. Ex vivo evaluation of the effects of compression on intestinal tissues. a) Von Mises stress values on tissues caused by capsule attraction through MM layouts with increasing magnet dimensions. b) 3D contour plot depicting von Mises stress and tissue squeezing with D22MM. c) Depiction of the setup used to perform a compression test on ex vivo tissues. d) Image of the ex vivo test, and close-up of samples colored with Indian Ink after being subjected to compression for 10 s and 2 min. e) Histological images of the sample after different time-points, including images of negative and positive controls. f) Damage score assigned by clinicians to histological images corresponding to tissues excised from two different donors (Test 1 and Test 2) for the different time-points and the positive control.

of our approach, which would result in a pressure on the intestinal tissue of about 63 kPa for less than 2 min.

The assessment of intestinal tissue trauma after applying stress has been the object of a few studies in humans and animals.[80–82] However, the large variability of protocols and tissues makes it difficult to identify a single damage threshold. Some studies identified 180 kPa as the minimum threshold to observe irreversible trauma on tissues on porcine.[82] Other works set it at 350 kPa in humans.[83] However, no studies analyzed the effects of a load over different time intervals. The observed minimal mucosa damage aligns with previous studies investigating stress-related tissue trauma. The consideration of villi and crypt length, morphology, and the preservation of the epithelial layer provided indices of damage.[84,85] These results provide insights into the correlation between the time during which a static load is applied and the resulting damage to freshly excised ex vivo human intestinal tissues.

2.4. Punching System: Needle Dimensioning

In order to transfer the drug from the capsule to the implanted reservoir, a punching unit is required. It comprises a needle and mechanism that allows it to move forward and enter the docked capsule. Two commercially available needle sizes- 27 G (Outer diameter 0.413 mm, inner diameter 0.21 mm) and 25 G (outer diameter 0.515 mm, inner diameter 0.26 mm) were evaluated. These sizes were chosen as a trade-off between insulin flow (lower needle inner diameter, higher pressure needed for aspiration), punching force, and the potential impact on the repeatedly punched intestine (outer diameter). To ensure the safety of the implant during the refilling procedure, taking into account the potential impact on the intestine tissue from repeated punching and the long lifespan of the implant, it was deemed impractical to use a needle size larger than 25 G.[86] Besides the needle size, the needle tip was selected with a non-coring feature to minimize the damage to the tissue and self-sealing septum that needs to be placed inside the device to prevent fluid leakage.[87,88] The 27 G needle was selected as the system's final needle because it produced significantly lower punching force than the 25 G needle and had a smaller diameter. Flow rate measurements and the evaluation of the impact of repeated tissue punching fall outside the scope of this paper. Future studies are warranted to investigate these aspects, particularly concerning conditions like T1D, where the disease significantly influences factors such as intestinal permeability and tissue integrity.[89–91]

2.5. Mechatronic Components

2.5.1. Roto-Translation Mechanism for Moving the Magnets

A mechanism allowing the magnetic units to switch from ON to OFF condition was designed based on the magnet dimensions and layout selected in Section 2.3. For each magnetic unit (top or bottom), a planetary gear mechanism was used to allow the roto-translation of the magnet. The planet gears were tied to the magnet planar faces and engaged with the sun gears, which in turn were directly connected to the motor. The magnets (through its planets' gears) moved along the ring gears, constrained to the

wall of the device case. The mechanism is shown in **Figure 5**a (left). A DC micromotor (Faulhaber, 1512U003SR324:1 IE2-8) was used to actuate the sun gears (16 teeth, module: 0.4); the planet gears held 54 teeth. For each magnetic unit, all the engaging gears were doubled to improve stability and avoid any misalignment due to the interaction of the magnets. A pin slot constraint also supported the roto-translation movement (Figure 5a, right).

2.5.2. Needle Linear Actuation

The 27 G needle was actuated by a rack-pinion mechanism (pinion gear 28 teeth, module 0.5) driven by a DC micromotor (Faulhaber, 1512U003SR324:1 IE2-8), as shown in Figure 5b.

2.5.3. Sensors

Capsule Arrival Sensor: Detecting the capsule arrival is desirable, thus activating the bottom magnetic circuit when the capsule is in the proximity of the device. An inductive proximity sensor was selected due to its selectivity to detect the metallic rings embedded in the capsule independently from the presence of tissue layers or digestion products. Sensor characterization showed that 6 mm was the maximum distance at which the sensor detected the capsule without being affected by the velocity of the capsule approaching. Considering the tissue thickness and the device wall, this distance was sufficient as a detecting range (more details about the characterization of the sensor can be found in Section S1 and Figure S12a,b, Supporting Information).

The sensor response was recorded while the capsule approached the device at different velocities from 0.5 to 20 mm s^{-1} (Figure S12c, Supporting Information). The sensor exhibited good reactivity when the rings passed in front of its active surface while transitioning to a stand-by mode once the non-metallic body of the capsule moved across its field (Figure S12d, Supporting Information). The sensor response to the capsule approaching with velocities of 0.5 and 1 mm s^{-1} is depicted in Figure 5c. As shown, the duration of the sensor's active state for the bottom and top rings depended on the velocity at which the capsule approached; higher velocities corresponded to shorter active times. This allowed the identification of a relationship between the sensor response time and the capsule velocity, as depicted in Figure 5d. By recording the inductive sensor response time, it was possible to estimate the velocity of the capsule due to the peristaltic action, which cannot be predicted a priori, since it is featured by a wide range of values, from basic peristalsis corresponding to 1–2 cm min^{-1} to rush peristalsis, corresponding to 2 cm s^{-1}.[92] Velocity estimation allows to impose a delay time after capsule detection before activating the bottom docking unit. This delay allows for proper alignment of the bottom ring of the capsule with the corresponding bottom magnet. The characterization of this sensor is a novelty with respect to the previous version of the device, which relied on magnet activation immediately after ingestion.[23] The possibility to monitor the capsule arrival constitutes a checkpoint on the procedure correctness; furthermore, it allows, in perspective, to explore the use of electromagnets, which could be activated only for a short time corresponding to capsule arrival. Finally, the possibility to estimate intestinal motility through the
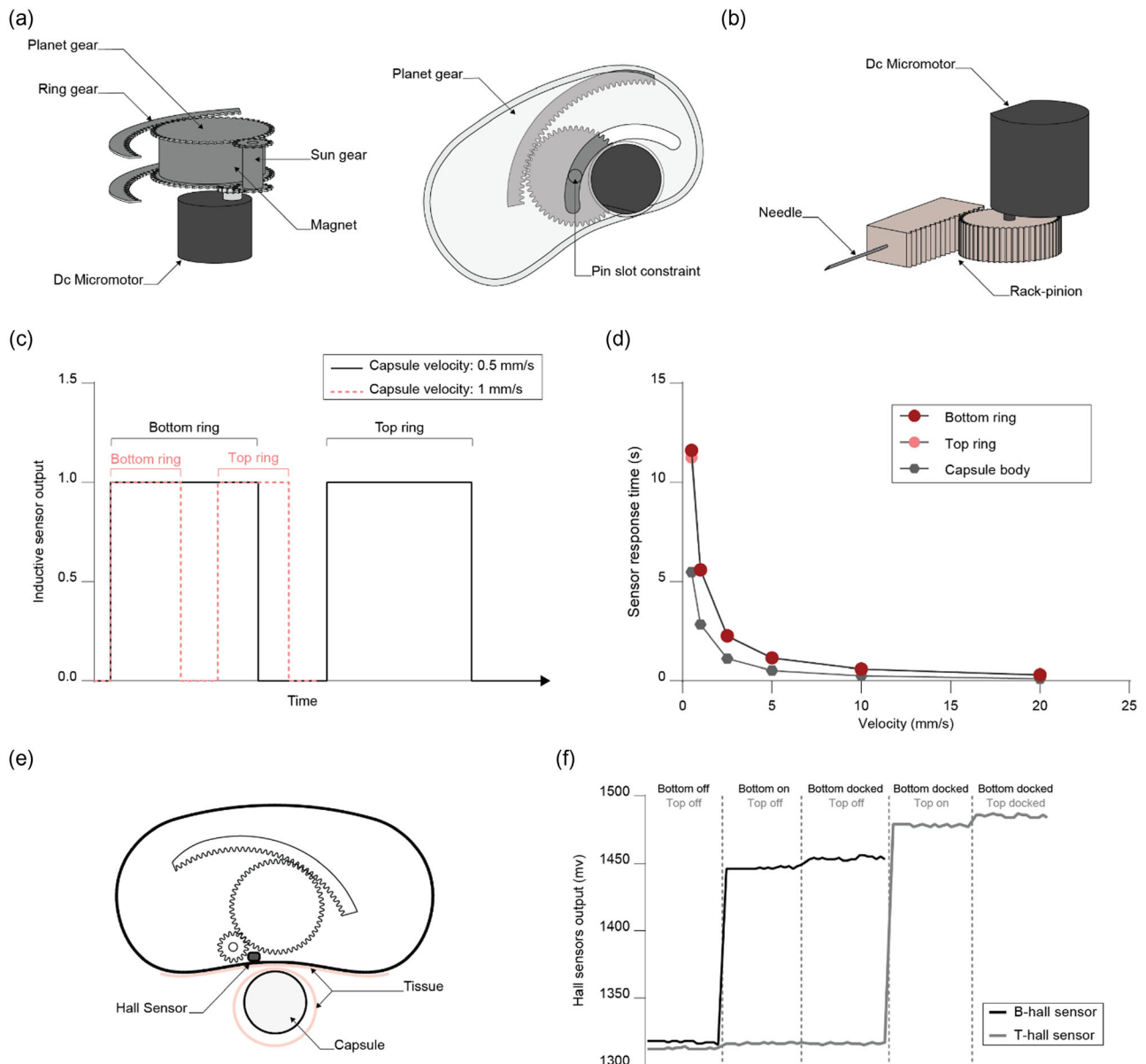
Figure 5. Mechatronic system components. a) Mechanism for activating the docking units: on the left, the planetary mechanism components are shown; they enable the magnet's roto-transitional movement; on the right, the gears integrated within the device to facilitate activation are represented. b) Punching system components. c) Output of the inductive sensors during detection of the bottom and top rings and capsule body at two velocities: 0.5 and 1 mm s⁻¹. d) Relationship between inductive sensor response time for different velocities for the top and bottom rings and capsule body. e) Top view of the device cross-section showing the Hall effect sensor position with respect to the device and the capsule. f) Output of the top and bottom Hall effect sensors during various activation steps of the docking units. B = bottom; T = top.

subsequent identification of the capsule rings opens to other possible applications in which ingestible devices may benefit from a synchronization between their functionality and the peristalsis activity level.

Docking Sensors: Two analog Hall effect sensors (Sonnecy, CYSJ902, Germany) were used to monitor the docking phases and allow the magnetic units' sequential activation. Each sensor, one per magnetic unit, was placed within the device wall between the magnet and the corresponding ring (top or bottom), as reported in Figure 5e. At this position, the magnetic field

variation sensed by the Hall effect sensors was more substantial with respect to other positions. Both sensors were used to: i) recognize the magnetic unit switch from the OFF to the ON condition and vice versa; ii) recognize the presence of the capsule ring when docked. After assembly within the docking system, the sensors were calibrated; the calibration results are shown in Figure 5f. When the bottom magnetic unit transited from the OFF-to-ON condition, the average output of the bottom Hall sensor was 130 mV, while the changes from the ON-to-dock condition were sensibly lower, 7 mV. The top Hall effect sensor

responded similarly: it showed 162 mV average changes when the top magnetic unit transitioned from OFF-to-ON, and only 7 mV average changes when the top ring docked relative to the ON condition. The outputs of the Hall effect sensors were used as a recognition routine implemented in the microcontroller (Atmega32, Microchip, USA) to handle the phases of the refilling procedure.

2.6. Device Assembly and Bench Tests

Following the individual testing of each component within the system, the subsequent phase involved the process of integration and assembly. As illustrated in **Figure 6**a, the assembled system included the inductive sensor, the docking system with magnetic units, the Hall effect sensors, and the punching system.

The firs*t* test assessed the reliability of the magnetic attraction generated by the docking system on the capsule with respect to the punching force. The capsule body was cut to show its internal structure and then manually placed in correspondence to the docking system in the ON condition. A silicone intestine model (wall thickness = 3.5 mm) was used to resemble the tissue thickness between the capsule and the device. Once the capsule was correctly placed, the punching system was activated, allowing the needle to punch the intestine model and the capsule wall. The footage of this test, in which the device was placed vertically along the gravity force, is shown in Movie S7, Supporting Information. The test was repeated with various orientations, demonstrating that the punching force did not affect the docking stability. Also, the gravity force did not influence the stability of the capsule docked by the magnets (Figure 6b). The efficiency of this system was assessed by conducting the test five times for each of the three orientations (horizontal, vertical, and lateral). A success rate of 100% was achieved in a total of 15 trials.

A second test was performed to demonstrate the capability of the bottom magnetic unit to effectively stop the capsule's navigation while withstanding the peristaltic force. For this purpose, a dedicated setup was built in which the capsule was pulled by a cable constrained to a linear guide. This cable was made of two segments connected magnetically through two hollow cylindrical magnets. The placement of the two magnets at a separation distance of 3 mm generated a pulling force of 0.53 ± 0.05 N, closely mirroring the axial component of the peristaltic force.[78] A scheme of this test is shown in Figure 6c. After the capsule was drawn toward the bottom unit, the successful disconnection of the two magnets in the cable confirmed that the docking force exerted by the bottom unit was strong enough to stop the capsule's movement, being higher than the peristaltic force as shown in Figure 6d. This qualitative observation was confirmed quantitatively by measuring the axial force necessary to detach the capsule from the bottom unit, which surpassed the peristaltic force (0.93 ± 0.10 N, velocity: 1 mm s^{-1}). Also, this test was repeated for different capsule dragging velocities as shown in Movie S8, Supporting Information; the capsule was successfully docked for the whole dragging velocity range (slow: 0.5, 1 mm s^{-1}, high: 5, 10, 20 mm s^{-1}) based on delay imposed on the bottom unit to avoid any misalignment between the magnet and the ring.

Finally, a test was conducted to demonstrate the device's ability to sequentially activate the refilling system components, thereby facilitating the docking, punching, and subsequent release of the capsule upon completion of the refilling procedure. The detailed workflow driving these steps is shown in Figure 6e. The complete cycle, with dragging velocities set at 5 mm s^{-1}, is shown in Movie S9, Supporting Information. A representative photo of the test is shown in Figure 6f. Three repetitions were conducted for each velocity, resulting in a total of 15 trials for five different velocities. The overall success rate was 93%, with some efficiency losses observed at a velocity of 20 mm s^{-1}.
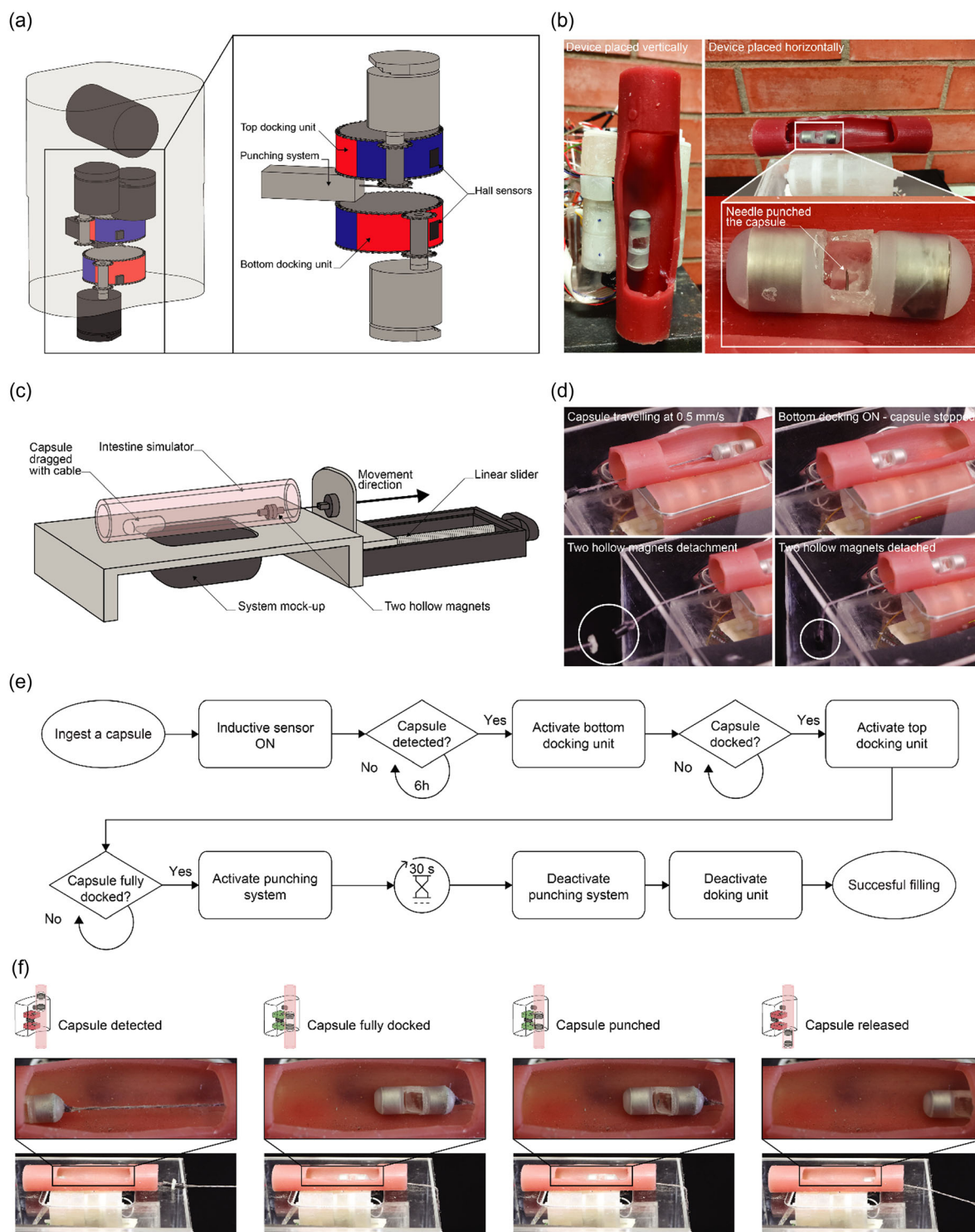
2.7. Chronic In Vivo Test of Punching System

To bridge the gap between bench testing and chronic in vivo evaluation and to circumvent the premature implementation of the entire complex system, we conducted a six-week implantation study in porcine models using a simplified version of the device. This streamlined implant included only the punching unit and the necessary electronic components for remote activation (**Figure 7**a–c) (additional details are described in the Experimental Section), while omitting the complete refilling system with the docking mechanism and capsule structure, which warrants dedicated future investigations.

The objectives of this chronic in vivo study were threefold: i) to assess the efficacy of the surgical techniques adopted to implant the device, which had only been evaluated for a single day in previous work;[28,31] ii) to examine the safety of the implantation procedure over a six-week period; and iii) to investigate the impact of the implantation process and the device's external casing on living tissue, an aspect not addressed in prior studies. Such an evaluation encompassed several vital aspects, including i) investigating the effects of the surgical procedure on gastrointestinal peristaltic functions in the short- and in the long-term; ii) monitoring the overall animal health over time; iii) assessing the impact of the implant on the surrounding intestinal tissue; iv) testing the sealing efficiency of the implanted device; and v) evaluating the functionality of electronic components and wireless communication, over the tested period. Continuous monitoring of the device's performance was carried out throughout the study period, assessing battery status, humidity levels, and the operation of electronic components within the in vivo environment.

Initially, the authors also aimed to assess the safety of repeated punching exerted by the needle on the intestinal tissues. However, as described below, this aspect could not be entirely evaluated.
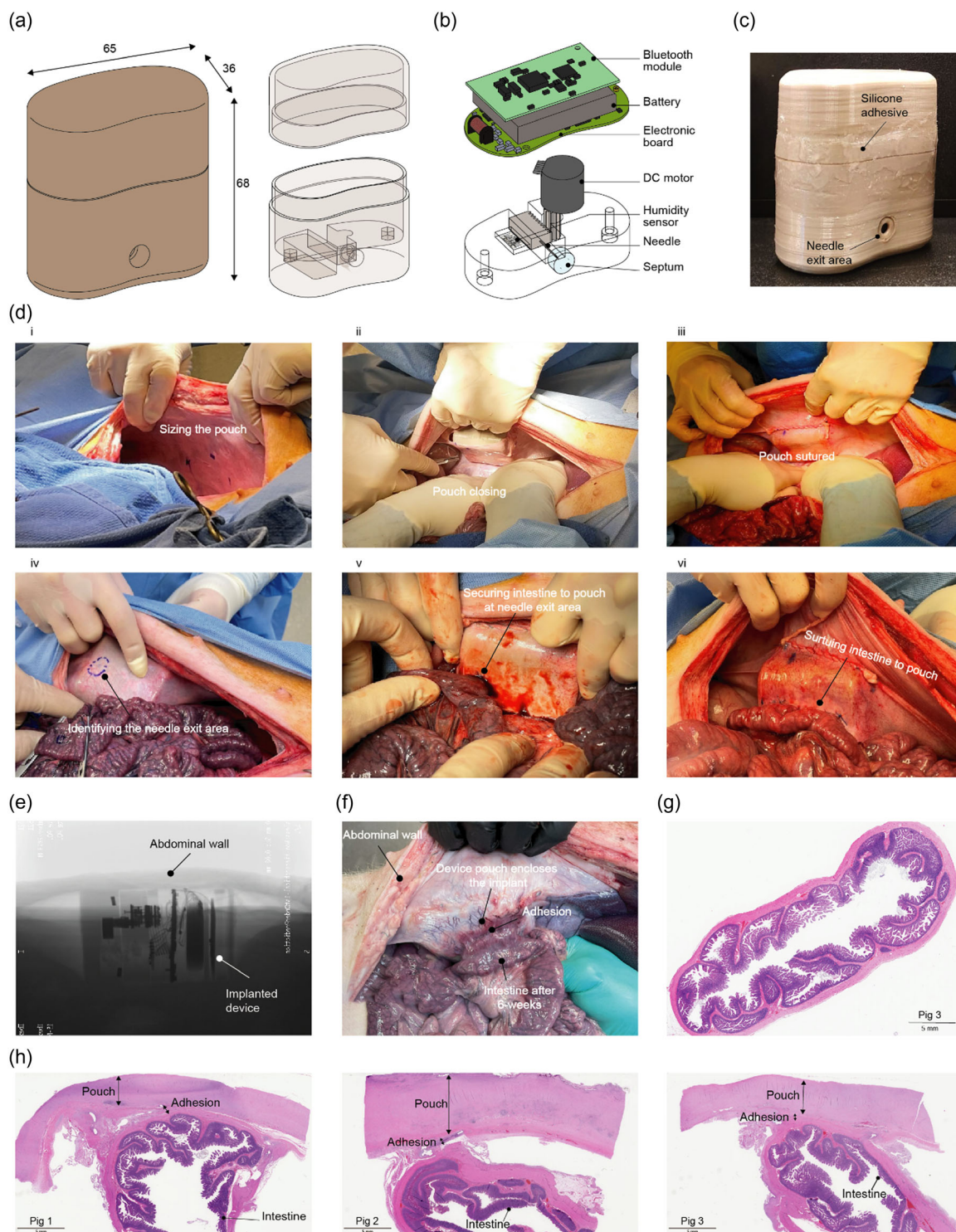
2.7.1. Device Implantation

The porcine model was chosen for this study due to its similarity to humans in terms of size, intestinal function, and morphology,[83,84] facilitating the translation of surgical procedures. Implantation was performed via a midline laparotomy to access the intraperitoneal area. An extraperitoneal pouch was bluntly dissected on the right abdominal wall to accommodate the device, ensuring minimal dead space (Figure 7d-i). The device was placed within the pouch and secured using non-absorbable nylon 2-0 sutures (Figure 7d-ii-iii). A loop from the third jejunum was selected and approximated to the device's concave side. The region directly over the needle exit area was secured first (Figure 7d-iv,v),

**ADVANCED
SCIENCE NEWS**

www.advancedsciencenews.com

**ADVANCED
INTELLIGENT
SYSTEMS**
Open Access

www.advintellsyst.com

Figure 6. System integration and outcomes of bench tests. a) CAD representation of the integrated system (left) and magnified view highlighting the docking and punching units (right). b) Image of the device placed at various orientations, with the fully docked capsule, to evaluate the punching event reliability and the impact of gravity on capsule stability. c) Setup was used to test the docking stability at different velocities. d) Images depicting the primary steps involved in testing docking stability at a velocity of 0.5 mm s^{-1}. e) Overall workflow of the control system. f) Images illustrating the main phases of the mechatronic system activation during a complete refilling cycle, including capsule detection, docking, punching, and deactivation to release the capsule.

ADVANCED
SCIENCE NEWS
www.advancedsciencenews.com

ADVANCED
INTELLIGENT
SYSTEMS
Open Access
www.advintellsyst.com

Figure 7. Implantable system components and outcomes of chronic in vivo tests. a) CAD representation of the assembled device (left) and a transparent view of the two halves of the external case displaying its geometric features (right). b) CAD of the main components included in the system, showcasing the electronic components (top) and punching unit components (bottom). c) Image of the implanted device after assembly and sealing. d) Images depicting the primary steps of the surgical procedure of implanting the devices (i-vi). e) Fluoroscopic images of the implantable device used to verify its position. f) Images of the tissue during necropsy and before explanting the implanted device. g) Histology image of the intestine tissue taken from a loop far from the implanted device (control sample). h) Histology images of the tissue in contact with the device after six weeks of implantation, including the extraperitoneal pouch and intestine.

2400125 (16 of 21)

followed by fixation of the surrounding intestinal section using sutures (Figure 7d-vi). After securing the intestinal loop, the abdomen was closed using 0 sutures for the primary layer and 2-s0 sutures for the subcuticular and skin layers, with surgical glue applied to the incision.

Post-implantation, fluoroscopic imaging was performed to verify the correct device placement (Figure 7e). The animals were closely monitored for general health, fecal output, and appetite recovery. Throughout the six-week study period, no clinical signs of illness were observed, and all three porcine models exhibited normal weight gain (Table S4, Supporting Information) and defecation, indicating the safety of the surgical procedure and implant, and unimpaired peristaltic function. The implanted devices were activated every four days to measure battery status, and humidity levels and to activate the punching system. Humidity levels remained within acceptable limits throughout the study (Figure S13, Supporting Information), and the punching system correctly worked for the entire period: it was successfully activated even after device removal (Movie S10, Supporting Information).

2.7.2. Necropsy and Histology

At the study's conclusion, the animals were humanely euthanized, and the implanted devices were retrieved. Necropsy revealed that all animals tolerated the device placement, with successful anchoring of the intestinal wall to the pouch (Figure 7f), which is a pre-requisite for successful future testing of the capsule-based refilling procedure.

However, it was observed that the devices had shifted and rotated to varying degrees within the pouch. Histological analyses of the tissue in contact with the implant, including the abdominal wall, device pouch, and treated intestinal loop near the implantation site, revealed changes ranging from minimal to mild, most of which were considered non-adverse and likely associated with the implantation procedure and device movement. Untreated intestinal loops distant from the implantation site, serving as control samples, showed no signs of alterations (Figure 7g), indicating that the implantation procedure did not affect other areas. Similarly, the treated intestinal loop (sutured to the pouch) exhibited no signs of inflammation or morphological changes (Figure 7h). Notably, thickening of the pouch tissue and adhesion formation between the pouch and intestinal loop was observed, suggesting a non-negligible fibrotic reaction to the implanted device (additional details in Section S2, Supporting Information).

The overall procedure proved to be safe and did not adversely affect the animals' health and peristalsis. Repeated activation of the punching unit over the six weeks also proved to be safe and did not imply adverse phenomena. However, the device moved within the pouch; thus, most probably, tissue punching did not occur consistently at the same point. As a consequence, it cannot be claimed that repeated punching of the intestinal tissue at the same point is safe, chronically. This aspect will require further investigation. Future enhancements will be needed, such as incorporating anchoring points on the device to avoid its movement, reducing the surface roughness of the external case and possibly providing it with anti-fouling coatings (e.g., zwitterionic polymers[93]), to minimize fibrotic reactions, and ensure the long-term success of the refilling system.

The findings reported in this article constitute a foundation that paves the way to future extensive in vivo evaluations of the complete system, including the capsule docking and refilling components, in a realistic physiological environment. Such studies will be crucial in assessing the long-term effects of the implantation procedure and the device's presence on intestinal wall integrity and function, ultimately targeting the translation of this novel drug delivery system into the clinical practice.

3. Conclusion

In this work, we presented an optimized solution for refilling implanted devices through ingestible capsules. A novel, passive drug-carrying capsule with a layout compatible with industrial injection molding fabrication technique was described. The capsule ensured insulin stability, resistance to the gastrointestinal fluids, simple filling of the sealed capsule, and low punching force. TPE Kraiburg was selected as the optimal material for the capsule shell. A docking system based on two independent magnetic units was proposed, enabling successful capsule docking and undocking across a broad range of tissue thicknesses. Magnetic switchable magnets and moving magnets were compared, finding better performance for the moving magnets, which were able to stably dock the capsule even at 5.92 mm, using a magnet with a diameter of 22 mm. The docking procedure safety was evaluated by conducting ex vivo tests on freshly excised human intestinal samples, finding that the stress applied by the docked capsule does not compromise tissue integrity. Additionally, an integrated prototype was successfully fabricated and assembled, incorporating the docking and punching systems, as well as sensors for driving its operation. Stable docking of the capsule and subsequent punching were demonstrated, irrespective of the peristaltic velocity applied and the device orientation. Finally, chronic in vivo testing on three pigs using a simplified version of the implanted system revealed a safe surgical procedure and normal animal health with no impact on bowel peristaltic activity and no histological signs of inflammation or morphological changes after a six-week period. However, tissue thickening in the pouch was observed due to a non-negligible fibrotic reaction. Future work should focus on providing the system with anchoring points and preventing excessive fibrotic reactions. Future extensive in vivo tests will assess capsule integrity and evaluate the entire functionality of the refilling system, including docking and punching mechanisms and the needle. Although the primary focus of this study was a system thought to treat type 1 diabetes patients, the findings of this article can be helpful for researchers targeting other chronic diseases, benefiting from an implanted reservoir periodically refilled in a non-invasive way.

4. Experimental Section

Pre-designed capsule shapes made of TPE (Kraiburg, Versaflex, Nevifood) and PVC were fabricated by a company specialized in injection molding (SA.GE srl, Italy). These samples were used to conduct FTIR, degradation, insulin stability, and punching tests.

FT-IR Characterization: FTIR spectra were collected for the different capsule candidate materials using an IRAffinity-1S (IR) spectrometer with an ATR module (Shimadzu) from 400 to 4000 cm^{-1} at 1 cm^{-1} resolution in 64 scans.

Preparation of Simulated Digestive Fluids: SGF and SIG were prepared according to USP (United States Pharmacopeia) specifications (Test Solutions, United States Pharmacopeia 35, NF 30, 2012) as reported in literature.[94]

Material Degradation Tests: Endoscopic capsules take ≈2 h to transit through the stomach, 6 h to pass through the small intestine, and up to 73 h to be excreted from the body, as evidenced by some clinical studies.[51,52] These values remain consistent in diabetic patients with irregular intestinal transit times.[95] In light of this information, a degradation test was conducted on the different capsule candidate materials. The materials were produced in small pieces and placed into 24 well plates (four independent samples for each material). Two mL of SGF and SIF were added, respectively, to different sets of samples. The plates were kept under continuous shaking at 37 °C for one day (for SGF) and five days (for SIF). An additional set of samples was treated sequentially with SGF for one day and SIF for five days. At the endpoint, samples were rinsed with water, left to dry for at least 24 h, and weighed. The change in mass was calculated as follows

$$\text{Mass ratio} = \frac{\text{final mass}}{\text{initial mass}} \tag{1}$$

Insulin Stability Tests: Three capsule bodies for each candidate material were filled with insulin (Insuman Infusat, 100 IU, Sanofi, France). Then, they were tightly closed to ensure the absence of air (which is known to favor insulin aggregation) and incubated at 37 °C under continuous shaking for 24 h. At the endpoint, three analytic techniques were used: i) turbidimetry tests were carried out with a LAMBDA 45 spectrophotometer (Perkin-Elmer Inc., USA), measuring the apparent absorbance of the samples at 350 nm by placing the insulin solutions in a 1 cm quartz cuvette. For each sample, the measurements were repeated three times. Deionized water was used as a blank, and limit of detection (LOD) was obtained as the mean value of the 350 nm absorbance of the blank plus three times its standard deviation (10 measurements); ii) dynamic light scattering measurements were performed with a Malvern Zetasizer Nano ZS analyzer. Each sample was measured three times with a scattering angle of 90°. The intensity distribution of particle sizes and volumes was recorded; iii) fluorescence measurements were conducted using an Agilent Cary Eclipse fluorescence spectrometer by monitoring the fluorescence intensity of Thioflavin T (ThT-50 µM, Sigma-Aldrich Corp., USA).[96] For the insulin test, the emission spectrum of 2 mL of ThT solution (solution A) was first measured by exciting the sample at 440 nm. Then, 20 µL of insulin was added to solution A (solution B), and the emission spectrum was measured using the same conditions. Three measurements were performed for each sample. The ratio of the fluorescence intensities of solution B and solution A at 490 nm was used to monitor insulin aggregation. A blank test was also performed by adding 20 µL of deionized water to solution A (blank). The LOD and LOQ (limits of quantitation) were obtained as the mean values of the ratio of fluorescence intensities of the blank and solution A plus three and ten times its standard deviation, respectively (ten measurements). Positive and negative controls were used for all three analytical techniques. The positive control consisted of fresh insulin taken from the original cartridges stored at 4 °C, as indicated by the manufacturer. As a negative control, denatured insulin was used. The denaturation was induced by incubating insulin at 37 °C for 24 h in the presence of 8 M urea and 1 M NaCl.[68,97]

Punching Tests: The force required to pierce the capsule shells was applied using dedicated 27 and 25 G non-coring needles (Hamilton, Romania). The needles were attached to a load cell (Nano17, ATI Industrial Automation, USA) that was linearly driven at 10 mm s^{-1} by a motorized linear stage (VT-80-100 mm, Physik Instrumente, GmbH, Germany). Three capsule shells were tested for each candidate material. For each shell, three punches were performed, repositioning the sample after each punch to avoid hitting the same point multiple times.

Testing of Self-Sealing Septum: Disc-shaped self-sealing septa made of silicon (Supelco, Sigma-Aldrich) with 11 mm diameter and 1.5 mm thickness were pierced with two 30 G non-coring needles (Hamilton, Romania) and then immersed in SGF for one day and SIF for five days (same conditions used to test the capsule materials). After the degradation test, the septa were inserted in a 3D-printed holder (VisiJet M3crystal, ProJet, MJP3600, 3D systems, U.S.A), as shown in Figure S4a, Supporting Information. The system was then filled with water supplemented with fluorescein (0.01 M). An increasing pressure was continuously applied through the syringe plunger. A pressure sensor (MPX5100DP, NXP Semiconductors, N.V., Netherlands) monitored the leakage from the holes created by the two needles. A white filter paper was inserted in the cap of the system. The pressure sensor was connected to an Arduino Uno board, and LabVIEW (National Instrument Corp., USA) was used for data acquisition. The experiment was repeated on four independent samples.

Capsule Fabrication: The mold for injection was made of steel, considering the materials' shrinkage tolerance of 1.8–2%. A "Baby-press" molding machine was used by SA.GE srl for capsule production. The nozzle and mold were kept at 175 and 13 °C, respectively. The injection pressure was 55 bar. No release agent was used.

Capsule Sealing: After fabrication, the capsule material was cleaned thoroughly with isopropyl alcohol to remove impurities on the material's surface. A cyanoacrylate medical adhesive (Loctite 4902, Henkel, Germany) was manually dispensed using a 5 mL syringe and general-purpose dispensing tips (Nordson EFD Corp., USA) with a size of 22 G. The adhesive was left to dry for at least one day before testing, as recommended by the manufacturer. A single lap joint was created using two layers of 6 × 30 × 0.6 mm (width × length × thickness) with a sealing overlap length of 6 mm (corresponding to the overlap length in the capsule structure, Figure S6a, Supporting Information). These layers were cut from the body of the fabricated capsule. An Instron tensile tester (Model 5900, 1 kN load cell) was used to measure the adhesion strength of the sealed components.

Leakage Test: The sealed capsule underwent dynamic loading through an adapter, namely a disc-shaped component having a diameter of 9.6 mm. The adapter was connected to a load cell (Nano 17, ATI Industrial Automation, USA) and actuated by a linear slider. A 3 s compression was repeatedly applied for more than 300 cycles. Throughout this procedure, continuous monitoring of the force sensor ensured that the applied force remained above 40 kPa. Subsequently, a resting period of 3 s followed. The compression focused on the capsule's central region, which is considered the weakest point in its body. This choice was made because the rigid ferromagnetic rings surrounding the capsule protected the other parts. The compression area reflected the length of the intestinal segment subjected to contraction, which typically ranges between 1 and 2 cm.[98]

Docking System Layouts: the docking system was based on two magnetic units aligned to the capsule's metallic rings. N52 diametrically magnetized permanent magnets (Algamagneti srl, Italy) were used for both solutions (MSD and MM), and commercial iron-nickel alloy (Alloy 50, Ed-Fagan Inc, UK) was used for the ferromagnetic components of the MSD solution.

Magnetic Simulation and Validation: MSD and MM solutions were compared using FE simulations. Before comparing the solutions, the selected magnets' grade was characterized in order to calibrate the magnetic properties to be set within the simulation environment. This characterization is described in Figure S8, Supporting Information. Five different permanent magnet diameters (22–26 mm) were considered; the height was fixed at 7 mm, as selected for the metallic rings inside the capsule. The AC-DC module of COMSOL Multiphysics v6 was used to perform the FE simulations. The force computed over the capsule rings was expressed as

$$F = \oint_{\partial \Omega} n_1 T_2 dS \tag{2}$$

where $\partial \Omega$ represents the boundary of the rings and $n_1 T_2$ is the normal component of the Maxwell stress tensor, defined as

$$n_1 T_2 = -\frac{1}{2}(H \times B)n_1 + (n_1 \times H)B^T \tag{3}$$

About 300 000 tetrahedral elements were used to mesh each model. A desktop computer holding eight cores processor and a 32 GB RAM was

**ADVANCED
SCIENCE NEWS**

www.advancedsciencenews.com

**ADVANCED
INTELLIGENT
SYSTEMS**
Open Access

www.advintellsyst.com

used to run the simulations (computational time: ≈2 min, mesh-convergent solution).

Experimental Validation of FE Simulations: To experimentally validate the FE simulation outcomes, a 3D-printed mockup of the device, including the bottom and the top MM units, was fabricated and fixed in correspondence with the capsule rings. The capsule was bound to a load cell (Nano17, ATI Industrial Automation, U.S.A) and mounted on a linear stage (VT-80-100 mm, Physik Instrumente, Germany). The attraction force was measured over different distances separating the magnetic docking unit and the capsule ring, thus obtaining results that could be compared with the simulation outputs.

FE Simulations of Tissue Compression Due to Capsule Docking: a multiphysics approach was pursued within COMSOL to estimate the coupled effect of the magnetic force attraction on the capsule and the compression of intestinal tissues interposed between the capsule and the docking unit. The Solid Mechanics module was used together with the AC-DC module to update iteratively the attraction force as the capsule squeezed the tissue in between. The problem was solved through a multi-component approach, using the *moving mesh* feature provided by the software. The force in Equation (2) was used step-by-step to solve the equation of motion (in the spatial formulation)

$$0 = \nabla_x \times \sigma + f_v \tag{4}$$

where σ is the Cauchy stress tensor and f_v is the volume force vector in the actual configuration. The capsule was modeled as a rigid body, while the intestine and the extraperitoneal pouch were modeled as hyperelastic materials. The intestine was modeled through the Mooney–Rivlin two-parameters strain energy function

$$W = C_{10}(I_1 - 3) + C_{01}(I_2 - 3) \tag{5}$$

where I_1, I_2 are the invariants and C_{10}, C_{01} are material parameters derived from the state-of-the-art.[99] The extraperitoneal pouch was modeled as a neo-Hookean material, and the parameters were extrapolated from the curves presented in a previous study.[100] the effect in terms of force and tissue compression was evaluated by considering five different magnet diameters, from 22 to 26 mm. For symmetry reasons, ¼ of the 3D model was considered.

Ex Vivo Intestinal Tissue Compression Experiments: The stress resulting from FE simulations was considered to design an ex vivo experiment on the small intestinal mucosa, evaluating the damage due to pressure applied for different periods. The freshly excised samples were derived from intestinal resection procedures carried out at Azienda Ospedaliero Universitaria Pisana, Cisanello (Pisa, Italy). After being subjected to compression, they were stored in 10% PBS buffered formalin and embedded in paraffin blocks. Some samples were used as negative control (no damage), while other samples were used as positive control (samples destroyed through a hammer bump). The average sample side size was 1 cm². Samples were subjected to 80 kPa for different time intervals (10 s, 2, 5 and 10 min). Samples of two different donors were analyzed for each time interval. Tissue analysis was performed by gastrointestinal pathologists after staining with formalin. Four µm-thick sections were cut, and the tissues were mounted on glass slides, then scanned at 400X and analyzed using an Aperio ImageScope (Leica Biosystems, Wetzlar, Germany). The analysis of the images enabled histopathologists to assign a score based on the extent of damage, categorized as no damage, superficial damage, intermediate damage, or deep damage. This score was correlated with factors such as residual villi and crypt lengths after compression, their morphology, and the preservation of the epithelial layer.[84,85]

Implantable Device Fabrication and Assembly: Three devices were fabricated for the in vivo testing using biocompatible poly-ether-ether-ketone (PEEK) material, which exhibits excellent mechanical properties and allows the development of complex shapes, such as the kidney-shaped design employed in our system, via 3D printing technology (Roboze SpA, Italy).[82] The device's external casing comprised two halves measuring $65 \times 36 \times 68$ mm³ with a wall thickness of 2.5 mm (Figure 7a). Within the casing, the punching system was assembled (Figure 7b) along with

an implantable self-sealing septum (MED-6215, Nusil) measuring 6 mm in length and 9 mm in diameter to prevent water intake. The electronic components included a customized electronic board with a microcontroller unit (STM32U575), a DC motor driver, and a humidity sensor (SHT40, Sensirion). A Bluetooth Low Energy module (Bluetooth 4.2) enabled reliable communication between the implanted device and the operator's phone. The device was powered by a compact 1100 mAh lithium-ion battery (Sena 1 °C, HXJNLDC) with a nominal voltage of 3.7 V. Following assembly and sealing (see below), the devices (Figure 7c) were sterilized using ethylene oxide before implantation.

Assembly and Sealing Process for the Devices Implanted In Vivo: the device surface underwent thorough cleaning with 70% ethanol. Then, the internal surface (excluding the bonding zone) was coated with a commercial conformal coating (419D Premium acrylic conformal coating, MG Chemicals) to prolong the implant's lifespan within the body. Indeed, plastic materials, including PEEK, have been observed to absorb humidity over time,[101] thus necessitating such a protective measure when long implantation times are targeted. Following the assembly of device components, starting with the punching system assembly and then the electronics, a silica gel was inserted to absorb humidity over time.[102] Then, the two halves of the case structure were closed. Following functionality testing, the sealing process started. A schematic sequence of the sealing procedure is depicted in Figure S14, Supporting Information: silicone adhesive was used to minimize moisture absorption. After complete adhesive curing over five days, the devices underwent ethylene oxide sterilization.

Animal Care and Surgical Procedure: The surgical procedure and the animal care both pre- and post-surgery, were conducted at IBEX Preclinical Research, Inc. in the USA.

Statistical Analyses: Statistical analyses were carried out using GraphPad Prism (v 8.0.2). A Kolmogorov-Smirnov normality test was performed on all experimental data to assess the type of data distribution. All data followed a normal distribution and were expressed as average values ± standard deviations. A one-way ANOVA was applied to evaluate statistical differences between experimental groups, followed by post-hoc analyses based on Tukey tests. The significance threshold was set at 0.05.

Supporting Information

Supporting Information is available from the Wiley Online Library or from the author.

Acknowledgements

Conflict of Interest

The authors declare no conflict of interest.

Keywords

[1] S. Bernell, S. W. Howard, *Front. Public Heal.* **2016**, *4*, 159.
[2] E. Meng, T. Hoang, *Adv. Drug Deliv. Rev.* **2012**, *64*, 1628.
[3] R. C. Bourge, A. B. Waxman, M. Gomberg-Maitland, S. M. Shapiro, J. H. Tarver, D. L. Zwicke, J. P. Feldman, M. M. Chakinala, R. P. Frantz, F. Torres, J. Cerkvenik, M. Morris, M. Thalin, L. Peterson, L. J. Rubin, *Chest* **2016**, *150*, 27.
[4] R. Sharma, D. Singh, P. Gaur, D. Joshi, *Drug Deliv. Transl. Res.* **2021**, *11*, 1878.
[5] S. H. Van Oostrom, R. Gijsen, I. Stirbu, J. C. Korevaar, F. G. Schellevis, H. S. J. Picavet, N. Hoeymans, *PLoS One* **2016**, *11*, 8.
[6] C. Jüngst, S. Gräber, S. Simons, H. Wedemeyer, F. Lammert, *QJM* **2019**, *112*, 505.
[7] B. Jimmy, J. Jose, *Oman Med. J.* **2011**, *26*, 155.
[8] F. P. Pons-Faudoa, A. Ballerini, J. Sakamoto, A. Grattoni, *Biomed. Microdevices* **2019**, *21*, 47.
[9] N. S. Wilcox, J. Rui, M. Hebrok, K. C. Herold, *J. Autoimmun.* **2016**, *71*, 51.
[10] V. Pathak, N. M. Pathak, C. L. O'Neill, J. Guduric-Fuchs, R. J. Medina, *Clin. Med. Insights. Endocrinol. Diabetes* **2019**, *12*, https://doi.org/10.1177/1179551419844521.
[11] P. Dandona, *Diabetes Technol. Ther.* **2017**, *19*, 498.
[12] C. Berget, L. H. Messer, G. P. Forlenza, *Diabetes Spectr.* **2019**, *32*, 194.
[13] N. D. Sora, F. Shashpal, E. A. Bond, A. J. Jenkins, *Am. J. Med. Sci.* **2019**, *358*, 326.
[14] L. Bally, H. Thabit, R. Hovorka, *Int. J. Pharm.* **2018**, *544*, 309.
[15] A. K. J. Gradel, T. Porsgaard, J. Lykkesfeldt, T. Seested, S. Gram-Nielsen, N. R. Kristensen, H. H. F. Refsgaard, *J. Diabetes Res.* **2018**, *2018*, https://doi.org/10.1155/2018/1205121.
[16] E. Renard, A. Farret, J. Place, in *Artif. Pancreas Curr. Situat. Futur. Dir.* Academic Press, Cambridge, MA **2019**, pp. 105–121.
[17] E. Dassau, E. Renard, J. Place, A. Farret, M.-J. Pelletier, J. Lee, L. M. Huyett, A. Chakrabarty, F. J. D. Iii, H. C. Zisser, *Diabetes Obes Metab* **2017**, *19*, 1698.
[18] I. Dirnena-Fusini, M. K. Åm, A. L. Fougner, S. M. Carlsen, S. C. Christiansen, *PLoS One* **2021**, *16*, 4.
[19] P. R. Van Dijk, S. J. J. Logtenberg, R. O. B. Gans, H. J. G. Bilo, N. Kleefstra, *Clin. Endocrinol.* **2014**, *81*, 488.
[20] R. Garcia-Verdugo, M. Erbach, O. Schnell, *J. Diabetes Sci. Technol.* **2017**, *11*, 814.
[21] M. L. Tanenbaum, S. J. Hanes, K. M. Miller, D. Naranjo, R. Bensen, K. K. Hood, *Diabetes Care* **2017**, *40*, 181.
[22] C. J. Witkowski, C. Saudek, *J. diabetes Sci. Technol.* **2008**, *2*, 703.
[23] L. Bally, H. Thabit, R. Hovorka, *Expert Opin. Drug Deliv.* **2017**, *14*, 1103.
[24] V. L. Ghafoor, M. Epshteyn, G. H. Carlson, D. M. Terhaar, O. Charry, P. K. Phelps, *Am. J. Heal. Pharm. AJHP Off. J. Am. Soc. Heal. Pharm.* **2007**, *64*, 2447.
[25] L. Ricotti, T. Assaf, A. Menciassi, P. Dario, in *2011 Annu. Int. Conf. IEEE Eng. Med. Biol. Soc.*, IEEE, Piscataway, NJ **2011**, pp. 2849–2853.
[26] L. Ricotti, T. Assaf, C. Stefanini, A. Menciassi, US9415163B2, **2016**.
[27] V. Iacovacci, L. Ricotti, P. Dario, A. Menciassi, *IEEE/ASME Trans. Mechatron.* **2015**, *20*, 1160.
[28] V. Iacovacci, I. Tamadon, E. F. Kauffmann, S. Pane, V. Simoni, L. Marziale, M. Aragona, L. Cobuccio, M. Chiarugi, P. Dario, S. Del Prato, L. Ricotti, F. Vistoli, A. Menciassi, *Sci. Robot.* **2021**, *6*, https://doi.org/10.1126/scirobotics.abh3328.
[29] Y. Sun, W. Zhang, J. Gu, L. Xia, Y. Cao, X. Zhu, H. Wen, S. Ouyang, R. Liu, J. Li, Z. Jiang, D. Cheng, Y. Lv, X. Han, W. Cai, E. Song, Q. Cao, L. Li, *Nat. Commun.* **2024**, *15*, 1839.
[30] S. S. Srinivasan, A. Alshareef, A. V. Hwang, Z. Kang, J. Kuosmanen, K. Ishida, J. Jenkins, S. Liu, W. A. M. Madani, J. Lennerz, A. Hayward, J. Morimoto, N Fitzgerald, R. Langer, G. Traverso, *Sci. Robot.* **202**, *7*, eabp9066.
[31] A. Abramson, M. R. Frederiksen, A. Vegge, B. Jensen, M. Poulsen, B. Mouridsen, M. O. Jespersen, R. K. Kirk, J. Windum, F. Hubálek, J. J. Water, J. Fels, S. B. Gunnarsson, A. Bohr, E. M. Straarup, M. W. Ley, X. Lu, J. Wainer, J. Collins, S. Tamang, K. Ishida, A. Hayward, P. Herskind, S. T. Buckley, N. Roxhed, R. Langer, U. Rahbek, G. Traverso, *Nat. Biotechnol.* **2022**, *40*, 103.
[32] A. Abramson, A. R. Kirtane, Y. Shi, G. Zhong, J. E. Collins, S. Tamang, K. Ishida, A. Hayward, J. Wainer, N. U. Rajesh, X. Lu, Y. Gao, P. Karandikar, C. Tang, A. Lopes, A. Wahane, D. Reker, M. R. Frederikse, B. Jensen, R. Langer, G. Traverso, *Matter* **2022**, *5*, 975.
[33] A. Abramson, E. Caffarel-Salvador, M. Khang, D. Dellal, D. Silverstein, Y. Gao, M. R. Frederiksen, A. Vegge, F. Hubálek, J. J. Water, A. V. Friderichsen, J. Fels, R. K. Kirk, C. Cleveland, J. Collins, S. Tamang, A. Hayward, T. Landh, S. T. Buckley, N. Roxhed, R. Langer, G. Traverso, *Science* **2019**, *363*, 611.
[34] A. Abramson, E. Caffarel-Salvador, V. Soares, D. Minahan, R. Y. Tian, X. Lu, D. Dellal, Y. Gao, S. Kim, J. Wainer, J. Collins, S. Tamang, A. Hayward, T. Yoshitake, H. Lee, J. Fujimoto, J. Fels, M. R. Frederiksen, U. Rahbek, N. Roxhed, R. Langer G. Traverso, *Nat. Med.* **2019**, *25*, 1512.
[35] S. Sarker, B. Wankum, T. Perey, M. M. Mau, J. Shimizu, R. Jones, B. Terry, *IEEE Trans. Biomed. Eng.* **2022**, *69*, 1870.
[36] M. Zhao, D. Liao, J. Zhao, *World J. Diabetes* **2017**, *8*, 249.
[37] J. B. Frøkjær, S. D. Andersen, N. Ejskjær, P. Funch-Jensen, A. M. Drewes, H. Gregersen, *World J. Gastroenterol.* **2007**, *13*, 4881.
[38] H. Al-Haddad, D. Guarnera, I. Tamadon, D. Luchetta, S. M. Isolani, C. Gianfaldoni, F. Vistoli, A. Menciassi, P. Dario, V. Iacovacci, L. Ricotti, *Proc. IEEE RAS EMBS Int. Conf. Biomed. Robot. Biomechatronics* **2022**, *2022*, https://doi.org/10.1109/biorob52689.2022.9925322.
[39] G. Cummins, *Adv. Drug Deliv. Rev.* **2021**, *177*, 113931.
[40] X. Wang, M. Q.-H. Meng, *Proc. Inst. Mech. Eng. Part H, J. Eng. Med.* **2010**, *224*, 107.
[41] D. Miley, L. B. Machado, C. Condo, A. E. Jergens, K.-J. Yoon, S. Pandey, *Adv. Devices Instrum.* **2024**, *2021*, https://doi.org/10.34133/2021/9854040.
[42] K. Kalantar-zadeh, N. Ha, J. Z. Ou, K. J. Berean, *ACS Sensors* **2017**, *2*, 468.
[43] P. A. Thwaites, C. K. Yao, E. P. Halmos, J. G. Muir, R. E. Burgell, K. J. Berean, K. Kalantar-Zadeh, P. R. Gibson, *Aliment. Pharmacol. Ther.* **2022**, *59*, 459.
[44] A. Abdigazy, M. Arfan, G. Lazzi, C. Sideris, A. Abramson, Y. Khan, *Nat. Electron.* **2024**, *7*, 102.
[45] K. Amellal, C. Tzoganakis, A. Penlidis, G. L. Rempel, *Adv. Polym. Technol.* **1994**, *13*, 315.
[46] L. W. McKeen, *Handb. Polym. Appl. Med. Med. Devices* **2014**, 21.
[47] C. Maier, T. Calafut, om *Polypropylene : The Definitive User's Guide And Databook*, Plastics Design Library division of William Andrew Inc., Norwich, NY, **1998**.
[48] R. Yang, in *Polym. Sci. Nanotechnol.* (Ed: R. Narain), Elsevier, Amsterdam **2020**, pp. 125–148.
[49] W. V. Titow, in *PVC Technology*, Springer Dordrecht, Dordrecht, The Netherlands **1984**.
[50] B. Gewert, M. M. Plassmann, M. Macleod, *Environ. Sci. Process. Impacts* **2015**, *17*, 1513.
[51] R. A. Hejazi, M. Bashashati, M. Saadi, Z. D. Mulla, I. Sarosiek, R. W. McCallum, M. J. Zuckerman, *Front. Med.* **2016**, *3*, 6.
[52] Y. Y. Lee, A. Erdogan, S. S. C. Rao, *J. Neurogastroenterol. Motil.* **2014**, *20*, 265.

**ADVANCED
SCIENCE NEWS**

www.advancedsciencenews.com

**ADVANCED
INTELLIGENT
SYSTEMS**
Open Access

www.advintellsyst.com

[53] A. Goldis, R. Goldis, T. V. Chirila, *Med.* **2019**, *55*, 734.

[54] How Enteral Feeding Tubes Affect Medicines – SPS - Specialist Pharmacy Service – The First Stop for Professional Medicines Advice, https://www.sps.nhs.uk/articles/how-enteral-feeding-tubes-affect-medicines/ (accessed: December, 2022).

[55] A. J. Weids, S. Ibstedt, M. J. Tamás, C. M. Grant, *Sci. Reports 2016 61* **2016**, *6*, 24554.

[56] K. D. Ratanji, J. P. Derrick, R. J. Dearman, I. Kimber, *J. Immunotoxicol.* **2014**, *11*, 99.

[57] L. Nielsen, R. Khurana, A. Coats, S. Frokjaer, J. Brange, S. Vyas, V. N. Uversky, A. L. Fink, *Biochemistry* **2001**, *40*, 6036.

[58] A. Nayak, A. K. Dutta, G. Belfort, *Biochem. Biophys. Res. Commun.* **2008**, *369*, 303.

[59] K. M. Bratlie, R. L. York, M. A. Invernale, R. Langer, D. G. Anderson, *Adv. Healthc. Mater.* **2012**, *1*, 267.

[60] S. Haghighi-Poodeh, L. Navidpour, P. Yaghmaei, A. Ebrahim-Habibi, *Biochem. Biophys. Res. Commun.* **2019**, *518*, 362.

[61] R. J. Woods, J. Alarcoń, E. McVey, R. J. Pettis, *J. Diabetes Sci. Technol.* **2012**, *6*, 265.

[62] H. C. Mahler, W. Friess, U. Grauschopf, S. Kiese, *J. Pharm. Sci.* **2009**, *98*, 2909.

[63] N. Sürmelioğlu, M. Nenni, A. Fırat, K. Demirkan, D. Özcengiz, *Int. J. Clin. Pract.* **2021**, *75*, e13895.

[64] L. Nault, P. Guo, B. Jain, Y. Bréchet, F. Bruckert, M. Weidenhaupt, *Acta Biomater.* **2013**, *9*, 5070.

[65] X. Bao, W. Li, M. Lu, Z. R. Zhou, *Biosurf. Biotribol.* **2016**, *2*, 49.

[66] L. J. Henze, N. J. Koehl, H. Bennett-Lenane, R. Holm, M. Grimm, F. Schneider, W. Weitschies, M. Koziolek, B. T. Griffin, *Eur. J. Pharm. Sci.* **2021**, *156*, 105627.

[67] F. Forouzandeh, N. N. Ahamed, M. C. Hsu, J. P. Walton, R. D. Frisina, D. A. Borkholder, *Micromachines* **2020**, *11*, 648.

[68] M. Muzaffar, A. Ahmad, *PLoS One* **2011**, *6*, e27906.

[69] C. Steiger, A. Abramson, P. Nadeau, A. P. Chandrakasan, R. Langer, G. Traverso, *Nat. Rev. Mater.* **2019**, *4*, 83.

[70] J. Byrne, H.-W. Huang, J. C. McRae, S. Babaee, A. Soltani, S. L. Becker, G. Traverso, *Adv. Drug Deliv. Rev.* **2021**, *177*, 113926.

[71] S. S. Srinivasan, A. Alshareef, A. V. Hwang, Z. Kang, J. Kuosmanen, K. Ishida, J. Jenkins, S. Liu, W. A. M. Madani, J. Lennerz, A. Hayward, J. Morimoto, N. Fitzgerald, R. Langer, G. Traverso, *Sci. Robot.* **2022**, *7*, eabp9066.

[72] N. Eliaz, *Materials* **2019**, *12*, https://doi.org/10.3390/ma12030407.

[73] G. Cummins, M. P. Y. Desmulliez, *Proc. Electron. Packag. Technol. Conf. EPTC*, IEEE, Singapore **2016**, *2016*, 407.

[74] D. Manas, M. Bednarik, A. Mizera, M. Manas, M. Ovsik, P. Stoklasek, *Polymers* **2019**, *11*, 1863.

[75] R. J. Saad, *Curr. Gastroenterol. Rep.* **2016**, *18*, 14.

[76] B. Guo, Y. Liu, S. Prasad, *Nonlinear Dyn.* **2019**, *98*, 3155.

[77] C. G. Cronin, E. Delappe, D. G. Lohan, C. Roche, J. M. Murphy, *Eur. J. Radiol.* **2010**, *75*, 207.

[78] H. Zhou, G. Alici, F. Munoz, *Biomed. Microdevices* **2016**, *18*, 102.

[79] H. Al-Haddad, I. Tamadon, D. Guarnera, A. Menciassi, P. Dario, A. Pfützner, F. Vistoli, V. Iacovacci, L. Ricotti, WO2023281428A1, **2021**.

[80] A. F. Khan, M. K. MacDonald, C. Streutker, C. Rowsell, J. Drake, T. Grantcharov, *BMJ surgery, Interv. Heal. Technol.* **2021**, *3*, e000084.

[81] W. Li, L. Shi, H. Deng, Z. Zhou, *Tribol. Lett.* **2014**, *55*, 261.

[82] S. De, J. Rosen, A. Dagan, B. Hannaford, P. Swanson, M. Sinanan, *Int. J. Rob. Res.* **2007**, *26*, 1159.

[83] A. F. Khan, M. K. Macdonald, C. Streutker, C. Rowsell, J. Drake, T. Grantcharov, *IEEE J. Transl. Eng. Heal. Med.* **2019**, *7*, 3300108.

[84] S. E. Mills, in *Sternberg's Diagnostic Surgical Pathology [6th Ed.]*, Wolters Kluwer Health, Baltimore, MD **2015**.

[85] J. F. Coleman, *Am. J. Surg. Pathol.* **2010**, *34*, 132.

[86] N. Di Trani, F. P. Pons-Faudoa, A. Sizovs, K. A. Shelton, M. A. Marzinke, P. N. Nehete, A. Grattoni, *Adv. Ther.* **2022**, *5*, https://doi.org/10.1002/adtp.202100214.

[87] R. Lo, P. Y. Li, S. Saati, R. N. Agrawal, M. S. Humayun, E. Meng, *Biomed. Microdevices* **2009**, *11*, 959.

[88] A. T. Evans, S. Chiravuri, Y. B. Gianchandani, *Biomed. Microdevices* **2010**, *12*, 179.

[89] E. Black, J. Vibe-Petersen, L. N. Jorgensen, S. M. Madsen, M. S. Ågren, P. E. Holstein, H. Perrild, F. Gottrup, *Arch. Surg.* **2003**, *138*, 34.

[90] M. Ø. Mønsted, N. D. Falck, K. Pedersen, K. Buschard, L. J. Holm, M. Haupt-Jorgensen, *J. Autoimmun.* **2021**, *122*, 102674.

[91] C. A. Thaiss, M. Levy, I. Grosheva, D. Zheng, E. Soffer, E. Blacher, S. Braverman, A. C. Tengeler, O. Barak, M. Elazar, D. Rotem Ben-Zeev, M. Lehavi-Regev, N. Katz, M. Pevsner-Fischer, A. Gertler, Z. Halpern, A Harmelin, S. Aamar, P. Serradas, A. Grosfeld, H. Shapiro, B. Geiger, E. Elinav, *Science* **2018**, *359*, 1376.

[92] L. Barducci, J. C. Norton, S. Sarker, S. Mohammed, R. Jones, P. Valdastri, B. S. Terry, *Prog. Biomed. Eng.* **2020**, *2*.

[93] D. Trel'ová, A. R. Salgarella, L. Ricotti, G. Giudetti, A. Cutrone, P. Šrámková, A. Zahoranová, D. J. Chorvát, D. Haško, C. Canale, S. Micera, J. Kronek, A. Menciassi, I. Lacík, *Langmuir* **2019**, *35*, 1085.

[94] J. Wang, V. Yadav, A. L. Smart, S. Tajiri, A. W. Basit, *Mol. Pharm.* **2015**, *12*, 966.

[95] A. Al hillan, D. Curras-Martin, M. Carson, S. Gor, A. Ezeume, V. Gupta, A. Copcaalvarez, G. Beri, M. Bermann, A. Asif, *Cureus* **2020**, *12*, https://doi.org/10.7759/CUREUS.6894.

[96] M. Schlein, *AAPS J.* **2017**, *19*, 397.

[97] A. Ahmad, I. S. Millett, S. Doniach, V. N. Uversky, A. L. Fink, *J. Biol. Chem.* **2004**, *279*, 14999.

[98] I. Sensoy, *Curr. Res. Food Sci.* **2021**, *4*, 308.

[99] C. Bellini, P. Glass, M. Sitti, E. S. Di Martino, *J. Mech. Behav. Biomed. Mater.* **2011**, *4*, 1727.

[100] E. J. White, E. M. Cunnane, M. McMahon, M. T. Walsh, J. C. Coffey, L. O'Sullivan, *Proc. Inst. Mech. Eng. Part H, J. Eng. Med.* **2018**, *232*, 796.

[101] N. Dahan, N. Donaldson, S. Taylor, N. Sereno, *J. Microelectron. Electron. Packag.* **2014**, *11*, 128.

[102] N. Dahan, N. Donaldson, S. Taylor, N. Sereno, *J. Microelectron. Electron. Packag.* **2013**, *10*, 15.